11-14-2013

A Production Efficiency Model-Based Method for Satellite Estimates of Corn and Soybean Yields in the Midwestern US

Qinchuan Xin
Tsinghua University, xqcchina@gmail.com

Peng Gong
University of California, penggong@berkeley.edu

Chaoqing Yu
Tsinghua University, chaoqingyu@gmail.com

Le Yu
Tsinghua University, leyu@tsinghua.edu.cn

Mark Broich
University of Technology Sydney, mark.broich@gmail.com

See next page for additional authors

Authors
Qinchuan Xin, Peng Gong, Chaoqing Yu, Le Yu, Mark Broich, Andrew E. Suyker, and Ranga B. Myneni

Joint control of terrestrial gross primary productivity by plant phenology and physiology

Jianyang Xia[a,1,2], Shuli Niu[b,1,2], Philippe Ciais[c], Ivan A. Janssens[d], Jiquan Chen[e], Christof Ammann[f], Altaf Arain[g], Peter D. Blanken[h], Alessandro Cescatti[i], Damien Bonal[j], Nina Buchmann[k], Peter S. Curtis[l], Shiping Chen[m], Jinwei Dong[a], Lawrence B. Flanagan[n], Christian Frankenberg[o], Teodoro Georgiadis[p], Christopher M. Gough[q], Dafeng Hui[r], Gerard Kiely[s], Jianwei Li[a,t], Magnus Lund[u], Vincenzo Magliulo[v], Barbara Marcolla[w], Lutz Merbold[k], Leonardo Montagnani[x,y], Eddy J. Moors[z], Jørgen E. Olesen[aa], Shilong Piao[bb,cc], Antonio Raschi[dd], Olivier Roupsard[ee,ff], Andrew E. Suyker[gg], Marek Urbaniak[hh], Francesco P. Vaccari[dd], Andrej Varlagin[ii], Timo Vesala[jj,kk], Matthew Wilkinson[ll], Ensheng Weng[mm], Georg Wohlfahrt[nn,oo], Liming Yan[pp], and Yiqi Luo[a,qq,1,2]

[a]Department of Microbiology and Plant Biology, University of Oklahoma, Norman, OK 73019; [b]Synthesis Research Center of Chinese Ecosystem Research Network, Key Laboratory of Ecosystem Network Observation and Modeling, Institute of Geographic Sciences and Natural Resources Research, Beijing 100101, China; [c]Laboratoire des Sciences du Climat et de l'Environnement, 91191 Gif sur Yvette, France; [d]Department of Biology, University of Antwerpen, 2610 Wilrijk, Belgium; [e]Center for Global Change and Earth Observations and Department of Geography, Michigan State University, East Lansing, MI 48824; [f]Climate and Air Pollution Group, Federal Research Station Agroscope, CH-8046 Zurich, Switzerland; [g]School of Geography and Earth Sciences, McMaster University, Hamilton, ON, Canada L8S 4K1; [h]Department of Geography, University of Colorado, Boulder, CO 80302; [i]European Commission, Joint Research Center, Institute for Environment and Sustainability, 21027 Ispra, Italy; [j]Institut National de la Recherche Agronomique, UMR 1137 Institut National de la Recherche Agronomique–Université de Lorraine, 54280 Champenoux, France; [k]Institute of Agricultural Sciences, Eidgenössische Technische Hochschule Zurich, 8092 Zurich, Switzerland; [l]Department of Evolution, Ecology and Organismal Biology, The Ohio State University, Columbus, OH 43210; [m]State Key Laboratory of Vegetation and Environmental Change, Institute of Botany, Chinese Academy of Sciences, Beijing 100093, China; [n]Department of Biological Sciences, University of Lethbridge, Lethbridge, AB, Canada TIK 3M4; [o]Tropospheric sounding, assimilation, and modeling group, Jet Propulsion Laboratory, Pasadena, CA 91109; [p]Institute of Biometeorology, 40129 Bologna, Italy; [q]Department of Biology, Virginia Commonwealth University, Richmond, VA 23284-2012; [r]Department of Biological Sciences, Tennessee State University, Nashville, TN 37209; [s]Civil and Environmental Engineering Department and Environmental Research Institute, University College Cork, Cork, Ireland; [t]Department of Agriculture and Environmental Sciences, Tennessee State University, Nashville, TN 37209; [u]Department of Bioscience, Aarhus University, 4000 Roskilde, Denmark; [v]Institute for Mediterranean Agricultural and Forest Systems, National Research Council, 80040 Ercolano, Italy; [w]Sustainable Agro-Ecosystems and Bioresources Department, Fondazione Edmund Mach, 38010 S. Michele all'Adige, Italy; [x]Servizi Forestali, Provincia Autonoma di Bolzano, 39100 Bolzano, Italy; [y]Faculty of Science and Technology, Free University of Bolzano, 39100 Bolzano, Italy; [z]Earth System Science and Climate Change Group, Wageningen University and Research Centre, Wageningen UR, 6700 AA Wageningen, The Netherlands; [aa]Department of Agroecology, Aarhus University, DK-8830 Tjele, Denmark; [bb]Department of Ecology, College of Urban and Environmental Sciences, Peking University, Beijing 100871, China; [cc]Key Laboratory of Alpine Ecology and Biodiversity, Institute of Tibetan Plateau Research, Center for Excellence in Tibetan Earth Science, Chinese Academy of Sciences, Beijing 100085, China; [dd]Institute of Biometeorology, National Research Council, 50145 Florence, Italy; [ee]Cirad-Persyst, UMR Ecologie Fonctionnelle and Biogéochimie des Sols et des Agro-Ecosystémes, 34060 Montpellier, France; [ff]Tropical Agricultural Centre for Research and High Education, 7170 Turrialba, Costa Rica; [gg]School of Natural Resources, University of Nebraska, Lincoln, NE 68583-0961; [hh]Department of Meteorology, Poznan University of Life Sciences, 60649 Poznan, Poland; [ii]A. N. Severtsov Institute of Ecology and Evolution, Russian Academy of Sciences, Moscow, 119071, Russia; Departments of [jj]Physics and [kk]Forest Sciences, University of Helsinki, FIN-00014 Helsinki, Finland; [ll]Centre for Sustainable Forestry and Climate Change, Forest Research, Farnham GU10 4LH, United Kingdom; [mm]Department of Ecology and Evolutionary Biology, Princeton University, Princeton, NJ 08544; [nn]Institute of Ecology, University of Innsbruck, 6020 Innsbruck, Austria; [oo]Institute for Applied Remote Sensing and Institute for Alpine Environment, European Academy of Bolzano, 39100 Bolzano, Italy; [pp]School of Life Sciences, Fudan University, Shanghai 200433, China; and [qq]Center for Earth System Science, Tsinghua University, Beijing 100084, China

Edited by William H. Schlesinger, Cary Institute of Ecosystem Studies, Millbrook, NY, and approved January 23, 2015 (received for review July 10, 2014)

Terrestrial gross primary productivity (GPP) varies greatly over time and space. A better understanding of this variability is necessary for more accurate predictions of the future climate–carbon cycle feedback. Recent studies have suggested that variability in GPP is driven by a broad range of biotic and abiotic factors operating mainly through changes in vegetation phenology and physiological processes. However, it is still unclear how plant phenology and physiology can be integrated to explain the spatiotemporal variability of terrestrial GPP. Based on analyses of eddy–covariance and satellite-derived data, we decomposed annual terrestrial GPP into the length of the CO_2 uptake period (CUP) and the seasonal maximal capacity of CO_2 uptake (GPP_{max}). The product of CUP and GPP_{max} explained >90% of the temporal GPP variability in most areas of North America during 2000–2010 and the spatial GPP variation among globally distributed eddy flux tower sites. It also explained GPP response to the European heatwave in 2003 (r^2 = 0.90) and GPP recovery after a fire disturbance in South Dakota (r^2 = 0.88). Additional analysis of the eddy–covariance flux data shows that the interbiome variation in annual GPP is better explained by that in GPP_{max} than CUP. These findings indicate that terrestrial GPP is jointly controlled by ecosystem-level plant phenology and photosynthetic capacity, and greater understanding of GPP_{max} and CUP responses to environmental and biological variations will, thus, improve predictions of GPP over time and space.

ecosystem carbon uptake | growing season length | photosynthetic capacity | spatiotemporal variability | climate extreme

Large variability exists among estimates of terrestrial carbon sequestration, resulting in substantial uncertainty in modeled dynamics of atmospheric CO_2 concentration and predicted future climate change (1). The variability in carbon sequestration is partially caused by variation in terrestrial gross primary productivity (GPP) (2), which is the cumulative rate over time of gross plant

Significance

Terrestrial gross primary productivity (GPP), the total photosynthetic CO_2 fixation at ecosystem level, fuels all life on land. However, its spatiotemporal variability is poorly understood, because GPP is determined by many processes related to plant phenology and physiological activities. In this study, we find that plant phenological and physiological properties can be integrated in a robust index—the product of the length of CO_2 uptake period and the seasonal maximal photosynthesis—to explain the GPP variability over space and time in response to climate extremes and during recovery after disturbance.

Author contributions: J.X., S.N., and Y.L. designed research; J.X. performed research; I.A.J., J.C., C.A., A.A., P.D.B., A.C., D.B., N.B., P.S.C., S.C., J.D., L.B.F., T.G., C.M.G., G.K., M.L., V.M., B.M., L. Merbold, L. Montagnani, E.J.M., J.E.O., A.R., O.R., A.E.S., M.U., F.P.V., A.V., T.V., M.W., G.W., and Y.L. contributed new reagents/analytic tools; J.X., D.H., L. Montagnani, and E.W. analyzed data; and J.X., S.N., P.C., I.A.J., J.C., C.A., P.D.B., A.C., D.B., N.B., S.C., L.B.F., C.F., T.G., C.M.G., D.H., G.K., J.L., M.L., V.M., B.M., L. Merbold, L. Montagnani, E.J.M., J.E.O., S.P., A.R., O.R., A.E.S., M.U., F.P.V., A.V., T.V., M.W., E.W., G.W., L.Y., and Y.L. wrote the paper.

The authors declare no conflict of interest.

This article is a PNAS Direct Submission.

[1]J.X., S.N., and Y.L. contributed equally to this work.

[2]To whom correspondence may be addressed. Email: jxia@ou.edu, sniu@igsnrr.ac.cn, or yluo@ou.edu.

This article contains supporting information online at www.pnas.org/lookup/suppl/doi:10.1073/pnas.1413090112/-/DCSupplemental.

photosynthesis at the ecosystem level. Plant photosynthesis has been successfully modeled at the biochemical level (3, 4). When leaf-level biochemical models of photosynthesis are scaled up to estimate annual GPP over a region and the globe, however, great uncertainty arises from both vegetation properties, such as biome-dependent leaf parameters (5, 6), and environmental factors, such as climate variability (7–9) and episodic disturbances (10–12). As a consequence, estimated present day global GPP varies from 105 to 177 Pg C y^{-1} in the fifth phase of the Coupled Model Intercomparison Project (13). Additionally, spatiotemporal patterns of GPP (2, 14), their responses to extreme climate events (12) and disturbances (10), and the underlying mechanisms are still not well-understood. Previous studies have indicated that vegetation properties and environmental factors shape annual GPP of an ecosystem directly or indirectly through affecting plant physiological activities (15) and/or phenology (16–21). Thus, integrating plant physiological and phenological properties may provide a unified approach to explain the variability of GPP over time and space and in response to disturbance.

In this study, we show that annual GPP in grams C meter^{-2} year^{-1}, the rate at which terrestrial ecosystems take up CO_2 from the atmosphere in a given year, can be quantitatively decomposed into

$$\mathrm{GPP} = \alpha \cdot \mathrm{CUP} \cdot \mathrm{GPP}_{\max}, \quad [1]$$

where the carbon dioxide uptake period (CUP; number of days per year) is a phenological indicator of the duration of ecosystem CO_2 assimilation within a given year. GPP_{max} (grams C meter^{-2} day^{-1}) is the maximal daily rate of gross photosynthesis during the CUP and represents a property of plant canopy physiology. The ratio between annual GPP and the product of CUP and GPP_{max} is represented by α. We estimated α, CUP, and GPP_{max} for 213 globally distributed terrestrial sites with daily GPP from the global network of micrometeorological tower sites (FLUXNET; La Thuile Database) (22) (*SI Appendix*, section S1.1.1 and Table S1) and all 0.1° × 0.1° land grid cells in North America during 2000–2010 with an 8-d GPP product from the Moderate Resolution Imaging Spectroradiometer (MODIS) onboard the National Aeronautics and Space Administration Terra satellite (23) (*Materials and Methods*). Here, we show how CUP and GPP_{max} jointly control the spatiotemporal variability of GPP and its response to and recovery from disturbances in different terrestrial ecosystems.

Results and Discussion

Using regression analysis, we first evaluated to what extent the product of CUP and GPP_{max} (CUP × GPP_{max}) explained the variability of satellite-derived GPP over broad temporal and spatial scales. CUP × GPP_{max} explained 94.9% of the interannual variability of the averaged MODIS GPP across North America from 2000 to 2010, with the minimum annual GPP (678 g C m^{-2} y^{-1}) in 2000 and the maximum (748 g C m^{-2} y^{-1}) in 2010 (Fig. 1*A*). The joint control of CUP and GPP_{max} on the interannual variability of GPP was robust in most MODIS grid cells across North America but weak in tropical and Mediterranean climates, such as the

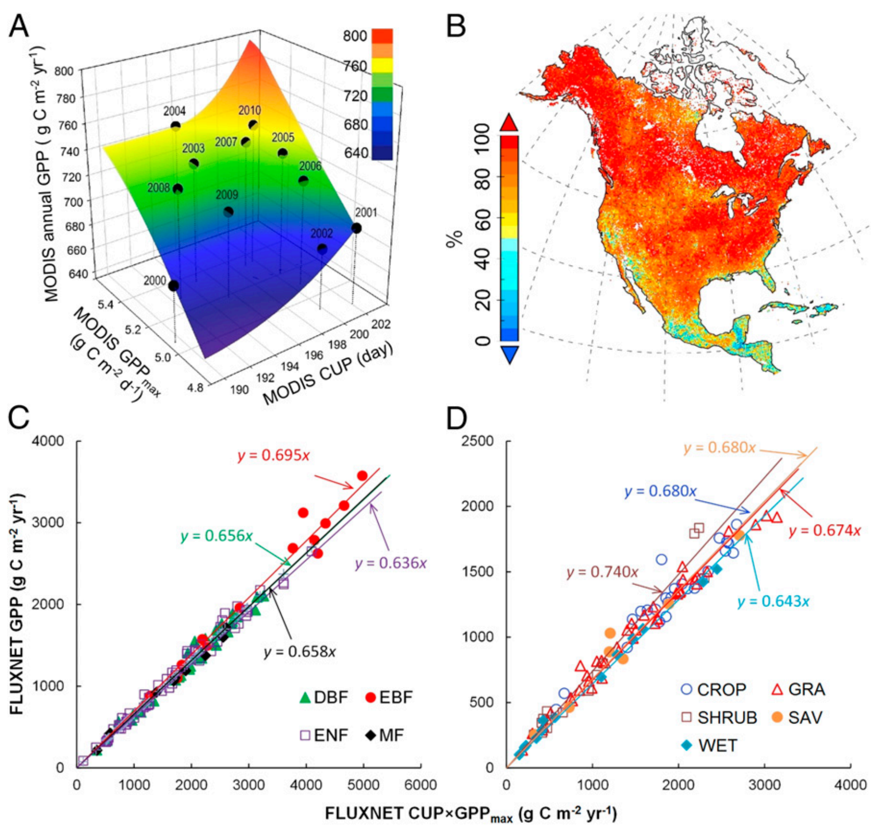

Fig. 1. Joint control of the temporal variability of satellite-derived annual GPP and the spatial variability of FLUXNET annual GPP by CUP and GPP_{max}. (*A*) The temporal variability of GPP in North America from 2000 to 2010 can be better understood by splitting annual GPP into GPP_{max} and CUP. The flat color interpolated surface reflects a good relationship between annual GPP and GPP_{max} × CUP (R^2 = 0.95, $P < 0.001$). Vertical lines were added to improve readability. (*B*) Contribution of GPP_{max} × CUP to GPP temporal variability over 2000–2010. The contribution in each grid cell was derived from the R^2 in the linear regression analysis between GPP and GPP_{max} × CUP. *C* and *D* show relationships between GPP and GPP_{max} × CUP across FLUXNET sites in forest and nonforest biomes, respectively. Each data point in *C* and *D* represents one flux site with average data over different years. CROP, cropland; DBF, deciduous broadleaf forest; EBF, evergreen broadleaf forest; ENF, evergreen needleleaf forest; GRA, grassland; MF, mixed forest; SAV, savanna; SHRUB, shrubland; WET, wetland.

Caribbean region and California (Fig. 1*B*). Spatially, across all FLUXNET sites, although there was no relationship between CUP and GPP_{max} (*SI Appendix*, Fig. S1), CUP × GPP_{max} explained >95% of the spatial variation of annual observed GPP in all biomes (all $P < 0.001$) (Fig. 1 *C* and *D*).

The product of CUP and GPP_{max} also explains the impact of a climate extreme on ecosystem CO_2 uptake. Linear regression analysis showed that the GPP reduction caused by the European heatwave in 2003 (12) across FLUXNET sites was well-explained by CUP × GPP_{max} ($R^2 = 0.90$, $P < 0.001$) (Fig. 2*A*, *Inset*). However, CUP and GPP_{max} played different roles in heatwave-induced GPP reduction among sites. For example, the reduction in annual GPP mainly resulted from a decrease of GPP_{max} (−37%) for a beech forest in Sarrebourg, France but a shortening of CUP (−11%) for a spruce site in Tharandt, Germany (Fig. 2*A*).

We also analyzed the dynamics of satellite-derived annual GPP, CUP, and GPP_{max} during recovery from a wildfire that occurred on August 24, 2000 in the Black Hills National Forest in South Dakota (24) (*SI Appendix*, Fig. S2). Although GPP_{max} and CUP followed contrasting postfire trajectories, the recovery trajectory of annual GPP was well-captured by the product of CUP and GPP_{max} ($R^2 = 0.88$, $P < 0.001$) (Fig. 2*B*). Immediately after the fire, GPP was sharply reduced by 27% in 2001 (624 g C m^{-2} y^{-1}) and 26% in 2002 (636 g C m^{-2} y^{-1}) relative to GPP before the disturbance in 2000 (858 g C m^{-2} y^{-1}). Thereafter, annual GPP gradually recovered to 816 g C m^{-2} y^{-1} in 2010 (Fig. 2*B*). The dynamics of GPP_{max} after the fire paralleled those of annual GPP, with 40% and 36% reduction in 2001 and 2002, respectively, and then gradual recovery to 89% of prefire levels in 2010. In contrast, the CUP was extended by 30 to 60 days from 2000 (219 d) and then gradually shortened and returned to predisturbance values (Fig. 2*B*). The rapid extension of the CUP may have resulted from the return of grass in spring after fire disturbance (25).

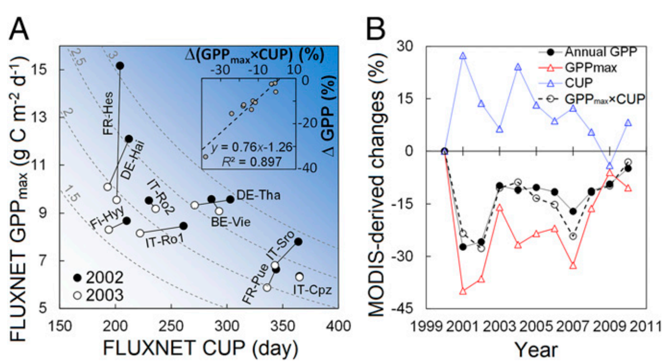

Fig. 2. Applications of the convergence of α (the ratio between annual GPP and GPP_{max} × CUP) to explain GPP response to and recovery from disturbances. (*A*) Determination of the annual GPP reduction during the European heatwave in 2003 (12) by GPP_{max} and CUP. The dashed hyperbolic curves represent constant values (shown near the curves) of GPP_{max} × CUP (kilograms C $meter^{-2}$ $year^{-1}$), and the darker background blue color means a larger GPP_{max} × CUP. *Inset* shows the dependences of the relative changes in annual GPP (ΔGPP; percentage) in 2003 from those in 2002 on the relative changes in GPP_{max} × CUP [Δ(GPP_{max} × CUP); percentage; black circles). The ten sites are: BE-Vie (Vielsalm, Belgium), DE-Hai (Hainich, Germany), DE-Tha (Tharandt, Germany), Fi-Hyy (Hyytiala, Finland), FR-Hes (Hesse Forest- Sarrebourg, France), FR-Pue (Puechabon, France), IT-Cpz (Castelporziano, Italy), IT-Ro1 and IT-Ro2 (Roccarespampani, Italy), IT-Sro (San Rossore, Italy). Detailed information about each FLUXNET site can be found in *SI Appendix*, Fig. S9 and Table S1. (*B*) Contrasting dynamics of GPP_{max} and CUP after an extensive wildfire in the Black Hills National Forest in South Dakota. The data were extracted from a burned 0.1° × 0.1° grid cell (43.85° N, 103.95° W) (original data are plotted in *SI Appendix*, Fig. S2). The ratio α was close to 0.62 during the 11-y span (*SI Appendix*, Fig. S10).

Not only did the product of CUP and GPP_{max} capture the variability in annual GPP over space and time and after disturbances, but the ratio α between annual GPP and CUP × GPP_{max} also converged across a broad range of vegetation types and environmental conditions (Fig. 3). The most frequent value of α was 0.62, with 90% of α-values falling within a range from 0.61 to 0.76 (Fig. 3*A*) based on an analysis of 213 FLUXNET sites. Those sites with $\alpha > 0.76$ were mainly located in tropical and subtropical climate zones (Fig. 3*A* and *SI Appendix*, Fig. S3). The analysis of the MODIS product showed a similar convergence of α over North America (Fig. 3*B*), with the most frequent value of 0.62 and a 90% range from 0.61 to 0.83. To explore the spatial distribution of α, we mapped the mean annual GPP, CUP, GPP_{max}, and α over 2000–2010. Although annual GPP, CUP, and GPP_{max} showed great spatial variability (*SI Appendix*, Fig. S4), α was relatively constant around 0.62 in most areas at a latitude of 37° N northward and gradually approached 1.0 toward the tropical regions of North America (Fig. 3*C*). Across North America, the temporal linear correlation between CUP × GPP_{max} and annual GPP was the highest in regions with α around 0.62 and gradually reduced with the ratio α approaching 1.0 (Fig. 3*D*).

High α-values were mainly distributed in tropical evergreen forest and regions with multiple growing seasons, where GPP_{max} and CUP exert weak controls over GPP variability (Fig. 3*A*, *Inset*). Values of α were high in tropical evergreen ecosystems, because GPP seasonality and amplitude were minimal, with plants assimilating CO_2 all year round. For example, daily GPP varied minimally across seasons in a tropical rain forest in Brazil (*SI Appendix*, Fig. S1.3.1), with α ranging between 0.77 and 0.80 from 2001 to 2003. The nontropical regions with high α-values usually have two or more peaks of daily GPP within a single year. For example, the Le Bray site in France, which is comprised of a maritime pine forest, had two separate GPP peaks in late May and September of 2005 (*SI Appendix*, Fig. S5). This phenomenon may also occur in Mediterranean regions with hot and dry summers (26) or double/triple cropping systems, where two or more crops are grown within a single year, such as winter wheat during winter and maize during summer in the North China Plain (27). Seasonally water-limited regions where two growing season peaks are present are widely distributed in the southern part of North America, leading to an abrupt increase in α at latitudes lower than about 30° N (Fig. 3*C*).

The decomposition of annual GPP into GPP_{max} and CUP allowed us to investigate the relative importance of GPP_{max} and CUP individually in regulating annual GPP variability among/within biomes (Fig. 4*A*). The linear correlation analysis across eight noncrop biomes showed that the biome-level GPP variability was significantly correlated to the variations in both GPP_{max} ($r^2 = 0.79$, $P = 0.003$) (Fig. 4*B*) and CUP ($r^2 = 0.64$, $P = 0.017$) (Fig. 4*C*). The partial correlation analysis across noncrop biomes revealed a larger contribution of GPP_{max} (partial $r^2 = 0.78$, $P = 0.004$) than CUP (partial $r^2 = 0.21$, $P < 0.001$) to GPP variability. A more important role of GPP_{max} than CUP in explaining the spatial variability of FLUXNET GPP was found within most biome types, including grassland (partial $r^2 = 0.70$, $P = 0.005$), shrubland (partial $r^2 = 0.52$, $P = 0.005$), savanna (partial $r^2 = 0.89$, $P = 0.001$), wetland (partial $r^2 = 0.91$, $P < 0.001$), and all forest types (partial $r^2 = 0.79$–0.87, all $P < 0.01$) (*SI Appendix*, Fig. S6 and Table S2). A recent analysis has found that temperature and precipitation changes impact the net primary productivity of woody plant ecosystems mainly through their effects on growing season length, standing biomass, and stand age (28). Thus, standing biomass and stand age might be very important determinants of GPP_{max} in forest ecosystems.

The joint control of GPP_{max} and CUP on GPP variability indicates that environmental changes influence annual GPP by simultaneously affecting vegetation phenology and photosynthetic capacity. For example, climate warming leads to greater ecosystem CO_2 uptake by extending CUP in most cold regions (7, 17, 29) but could reduce ecosystem CO_2 uptake when

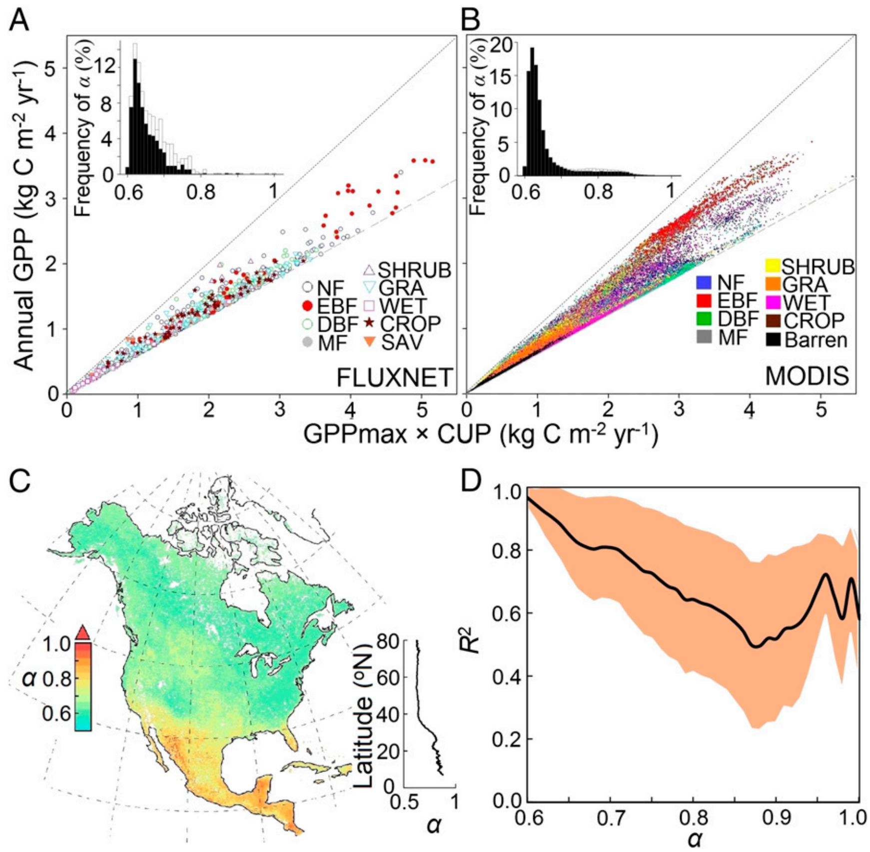

Fig. 3. The relationship between annual GPP and the product of CUP and GPP_{max} (i.e., α) from FLUXNET and satellite-derived data. The relationship between annual GPP and CUP × GPP_{max} is shown across (*A*) all FLUXNET site-years and (*B*) all 0.1° × 0.1° land grids in North America. *C* shows spatial distributions of satellite-derived α, and *D* shows the relationship between α and the explanation of GPP_{max} × CUP on temporal variability of annual GPP (R^2) (Fig. 1*B*) in North America. *A*, *Inset* and *B*, *Inset* show the relative frequency distribution of estimated α from all FLUXNET site-years and MODIS GPP data, respectively. The white bars are data from tropical and subtropical climate (including Mediterranean) zones and site-years with multiple GPP peaks, whereas the black bars are data from the rest of the site-years. *C*, *Inset* shows the latitudinal pattern of α with a 0.1° interval. CROP, cropland; DBF, deciduous broadleaf forest; EBF, evergreen broadleaf forest; GRA, grassland; NF, needleleaf forest; MF, mixed forest; SAV, savanna; SHRUB, shrubland; WET, wetland.

the GPP_{max} is suppressed by the reduced snow melt water in spring (30, 31). Similarly, a recent analysis showed that warming-induced earlier springs reduced summer peak productivity during 1982–2008 in the North American boreal forests (32), which may have contributed to the declining trend of vegetation productivity associated with the climatic warming at northern high latitudes in the past few decades (33).

Given that simulated global GPP and its sensitivity to environmental factors vary substantially among current terrestrial biosphere models (13, 34), the findings in this study suggest that such uncertainty could largely stem from the different representations of vegetation phenology and photosynthetic capacity in the models. For example, although numerous vegetation phenology models have been developed for different biomes over the past few decades (35, 36), some existing terrestrial biosphere models poorly represent vegetation phenology in North America (8). Moreover, in those models, vegetation photosynthetic capacity may be unrealistically limited by the fixed parameterization of maximum rate of carboxylation (37), with observations indicating substantial temporal and spatial variations in maximum carboxylation (38, 39). Broadly collected vegetation phenology data derived from observations (40, 41), remote sensing (42, 43), and digital repeat photography (44, 45) as well as additional mechanistic understanding of canopy photosynthetic capacity (39, 46–48) could be useful to diagnose or benchmark model performances of simulating GPP (49).

Because the GPP_{max} and CUP estimates were derived from existing data, our approach cannot be used for GPP prediction unless GPP_{max} and CUP can be inferred from other indicators. We first examined whether GPP_{max} derived from MODIS GPP data was comparable with that measured by the flux towers in North America. We found that, although the two datasets had different spatial and temporal scales, the GPP_{max} estimates from MODIS data were close to those from FLUXNET data at most sites with low GPP_{max} (*SI Appendix*, Fig. S7). The FLUXNET data had much higher GPP_{max} than MODIS data, mainly in the cropland sites with high GPP_{max} (*SI Appendix*, Fig. S7). In addition to FLUXNET data, the maximum monthly sun-induced chlorophyll fluorescence data could be useful to estimate GPP_{max} globally (50). We also examined whether the MODIS-derived CUP can be inferred from other types of satellite-derived datasets, such as the daily record of freeze/thaw status across North America (*SI Appendix*, section 1.8). We found that the MODIS-derived CUP is strongly correlated with the photosynthetically active period estimated from the freeze/thaw status data at most latitudes (*SI Appendix*, Fig. S8). The freeze/thaw status data can only provide information where the soil actually freezes in winter, partially leading to the disagreement between the two datasets in tropical regions (*SI Appendix*, Fig. S8). Thus, Eq. **1** could be useful for estimating and predicting annual GPP if both CUP and GPP_{max} can be inferred from biotic and abiotic drivers measured at a global scale, the topic of a substantial body of ongoing research (15, 51).

In summary, we found a simple proximate cause to explain variation in annual GPP (i.e., Eq. **1**) over space and time, in response to a climate extreme, and during recovery after disturbance.

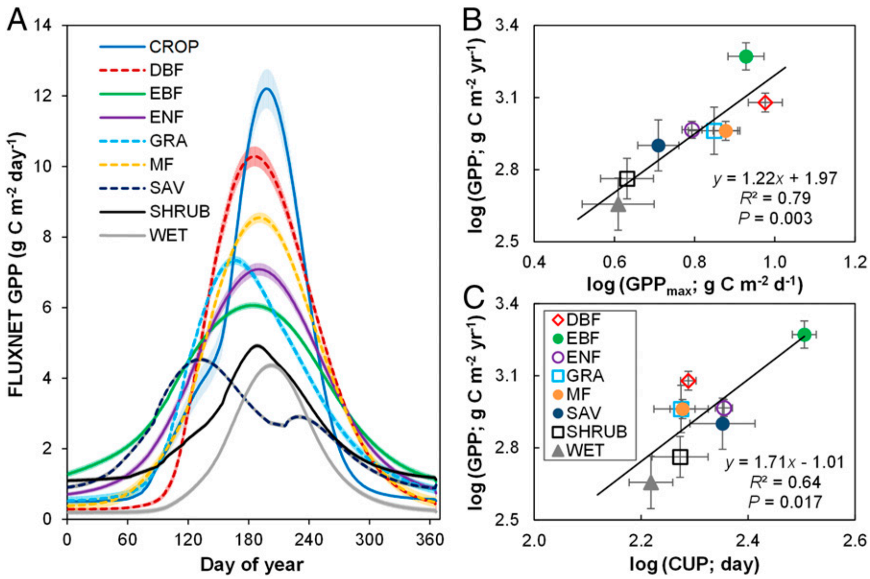

Fig. 4. (*A*) Dynamic of daily GPP in different biomes based on the FLUXNET dataset. The curves are obtained by averaging daily GPP over all site-years of each biome type, with the shaded areas representing SEs on GPP. *B* and *C* show dependence of annual FLUXNET GPP variability on GPP_{max} and CUP, respectively, among biomes. Note that cropland was excluded in the correlation analyses. Note that there were, in total, 12 EBF sites in this analysis, and 7 of them were distributed in the temperate zone according to the MODIS IGBP (International Geosphere-Biosphere Programme) land cover classification (glcf.umd.edu/data/lc/) (*SI Appendix*, Table S1). CROP, cropland; DBF, deciduous broadleaf forest; EBF, evergreen broadleaf forest; ENF, evergreen needleleaf forest; GRA, grassland; MF, mixed forest; SAV, savanna; SHRUB, shrubland; WET, wetland.

The representation of interannual and spatial variations in GPP by the product of CUP and GPP_{max} was strong in those ecosystems with α-values close to 0.62 but weaker toward the tropics or in seasonally water-limited regions, where α-values approached 1.0. The strong correlation of annual GPP with the product of CUP and GPP_{max} in several different ecosystem types may be useful in detecting shifts in vegetation state and for monitoring short- and long-term response of GPP to extreme climate conditions and disturbances. Given that GPP_{max} better explains GPP variability than CUP, future studies need to emphasize the regulatory mechanisms for the dynamics of ecosystem photosynthetic capacity in terrestrial ecosystems.

Materials and Methods

GPP estimates (positive GPP means CO_2 uptake) from 213 FLUXNET sites from the La Thuile Database (www.fluxdata.org/default.aspx) (*SI Appendix*, Table S1) and the MODIS aboard National Aeronautics and Space Administration Terra satellites (MOD17A2 GPP) (23) were used in the analyses (*SI Appendix*, section S1.1). For FLUXNET sites, only those site-years with >300 daily estimates were chosen from the database. Because the MODIS GPP product was well-evaluated in North America (52), we only performed our analysis on MODIS GPP in this region from 2000 to 2010.

The determinations of CUP and GPP_{max} were from the method introduced by Gu et al. (53, 54) (*SI Appendix*, section S1.2). The CUP, GPP_{max}, and the ratio between annual GPP and CUP × GPP_{max} (i.e., α) were estimated for each selected FLUXNET site and each 0.1° × 0.1° land grid cell of the MODIS product by the following steps (*SI Appendix*, section S1.3). (*i*) We judged if the site-year or grid cell is evergreen or not by counting the number of days with larger daily GPP than a given value (a site or land grid cell was defined as evergreen if there were more than 360 d with daily GPP > 1 g C m^{-2} d^{-1} within 1 y). (*ii*) The number of seasons in the nonevergreen site-years or land grid cells was determined by a model function (*SI Appendix*, section S1.3 and Eq. **S6**) suggested by the TIMESAT software (55). For those site-years and grid cells with one season, we fitted a five-parameter Weibull function to the data from that year. For those site-years or land grid cells with more than one season, we fitted the Weibull function to each season.

The nonlinear data fitting was performed with the function nls in R (www.r-project.org/) (*SI Appendix*, section S1.4). The robustness of the method was carefully validated by various approaches, including an evaluation with the data from all long-term FLUXNET sites (*SI Appendix*, section S1.5), a parameter sensitivity analysis of the Weibull function (*SI Appendix*, section S1.6), and a random resampling test of the Weibull function (*SI Appendix*, section S1.7). Linear regression analysis was used to examine the contribution of CUP × GPP_{max} to the temporal and spatial variations of annual GPP. The global daily record of landscape freeze/thaw data from January 1, 2000 to December 31, 2010 was analyzed for an additional indicator of CUP (*SI Appendix*, section S1.8).

To further identify the relative contribution of GPP_{max} and CUP to GPP variability, we first linearized Eq. **1** by replacing all variables with their logarithms (base 10) as

$$\log(GPP) = \log(\alpha) + \log(CUP) + \log(GPP_{max}). \qquad [2]$$

Then, we applied the partial correlation analysis to examine the relative contributions of CUP and GPP_{max} to FLUXNET GPP variability among and within biomes.

ACKNOWLEDGMENTS. We thank the anonymous reviewers and Steven Running for their constructive comments and suggestions, and Lianhong Gu and Ying-Ping Wang for their help in data analyses. The eddy covariance database used in this study was the outcome of the La Thuile FLUXNET (a global network of micrometeorological tower sites) Workshop 2007, which was supported by the Office of Science, US Department of Energy for AmeriFlux, CarboEuropeIP, FAP-GTOS-TCO (Food and Agriculture Project - Global Terrestrial Observing System - Terrestrial Carbon Observations), iLEAPS (Intergrated Land Ecosystem - Atmosphere Processes Study), NitroEurope, Max Planck Institute for Biogeochemistry, National Science Foundation, University of Tuscia, Universite Laval, and Environment Canada, and database development and technical support were from the Berkeley Water Center, the Lawrence Berkeley National Laboratory, and Microsoft Research eScience. The data were mainly acquired by the following networks: AmeriFlux (US Department of Energy, Biological and Environmental Research, Terrestrial Carbon Programs DE-FG02-04ER63917 and DE-FG02-04ER63911), GHG-Europe (Greenhouse gas management in European land use systems), SOERE (Système d'Observation et d'Expérimentation sur le long terme pour la Recherche en Environnement) FORE-T (Fonctionnement des écosystèmes forestiers) Fluxnet-Canada Research Network and Canadian Carbon Program (supported by CFCAS (Canadian Foundation for Climate and Atmospheric Sciences), NSERC (Natural Sciences and Engineering Council of Canada), BIOCAP (Biosphere Implications of CO2 Policy in Canada), Environment Canada, and NRCan (Natural Resources Canada), GreenGrass, KoFlux, LBA (Large-scale Biosphere-Atmosphere Experiment in Amazonia), NECC (North Equatorial Countercurrent), OzFlux, TCOS-Siberia (Terrestrial Carbon Observation System Siberia), and USCCC (US–China Carbon Consortium). This work was financially supported by US Department of Energy, Terrestrial Ecosystem Sciences Grant DE SC0008270 and National Science Foundation Grants DEB 0743778, DEB 0840964, EPS 0919466, EF 1137293, and IIA-1301789.

1. Graven HD, et al. (2013) Enhanced seasonal exchange of CO_2 by northern ecosystems since 1960. *Science* 341(6150):1085–1089.
2. Jung M, et al. (2012) Global patterns of land-atmosphere fluxes of carbon dioxide, latent heat, and sensible heat derived from eddy covariance, satellite, and meteorological observations. *J Geophys Res Biogeosci* 116:G00J07.
3. Farquhar GD, von Caemmerer S, Berry JA (1980) A biochemical model of photosynthetic CO_2 assimilation in leaves of C_3 species. *Planta* 149(1):78–90.
4. Collatz GJ, Ribas-Carbo M, Berry J (1992) Coupled photosynthesis-stomatal conductance model for leaves of C_4 plants. *Funct Plant Biol* 19(5):519–538.
5. Reich PB, Walters MB, Ellsworth DS (1992) Leaf life-span in relation to leaf, plant, and stand characteristics among diverse ecosystems. *Ecol Monogr* 62(3):365–392.
6. Cramer W, et al. (1999) Comparing global models of terrestrial net primary productivity (NPP): Overview and key results. *Glob Chang Biol* 5(S1):1–15.
7. Xia JY, et al. (2014) Terrestrial carbon cycle affected by non-uniform climate warming. *Nat Geosci* 7(3):173–180.
8. Richardson AD, et al. (2012) Terrestrial biosphere models need better representation of vegetation phenology: Results from the North American Carbon Program Site Synthesis. *Glob Chang Biol* 18(2):566–584.
9. Bellenger H, Guilyardi E, Leloup J, Lengaigne M, Vialard J (2014) ENSO representation in climate models: From CMIP3 to CMIP5. *Clim Dyn* 42(7-8):1999–2018.
10. Amiro BD, et al. (2010) Ecosystem carbon dioxide fluxes after disturbance in forests of North America. *J Geophys Res Biogeosci* 115(G4):G00K02.
11. Running SW (2008) Climate change. Ecosystem disturbance, carbon, and climate. *Science* 321(5889):652–653.
12. Ciais P, et al. (2005) Europe-wide reduction in primary productivity caused by the heat and drought in 2003. *Nature* 437(7058):529–533.
13. Anav A, et al. (2013) Evaluating the land and ocean components of the global carbon cycling in the CMIP5 Earth System Models. *J Clim* 26:6801–6843.
14. Beer C, et al. (2010) Terrestrial gross carbon dioxide uptake: Global distribution and covariation with climate. *Science* 329(5993):834–838.
15. Stoy PC, Trowbridge AM, Bauerle WL (2014) Controls on seasonal patterns of maximum ecosystem carbon uptake and canopy-scale photosynthetic light response: Contributions from both temperature and photoperiod. *Photosynth Res* 119(1-2): 49–64.
16. Xia J, Wan S (2012) The effects of warming-shifted plant phenology on ecosystem carbon exchange are regulated by precipitation in a semi-arid grassland. *PLoS ONE* 7(2):e32088.
17. Piao S, Friedlingstein P, Ciais P, Viovy N, Demarty J (2007) Growing season extension and its impact on terrestrial carbon cycle in the Northern Hemisphere over the past 2 decades. *Global Biogeochem Cycles* 21(3):GB3018.
18. Richardson AD, et al. (2010) Influence of spring and autumn phenological transitions on forest ecosystem productivity. *Philos Trans R Soc Lond B Biol Sci* 365(1555):3227–3246.
19. Keenan TF, et al. (2014) Net carbon uptake has increased through warming-induced changes in temperate forest phenology. *Nat Clim Chang* 4:598–604.
20. Churkina G, Schimel D, Braswell BH, Xiao X (2005) Spatial analysis of growing season length control over net ecosystem exchange. *Glob Chang Biol* 11(10):1777–1787.
21. Dragoni D, et al. (2011) Evidence of increased net ecosystem productivity associated with a longer vegetated season in a deciduous forest in south-central Indiana, USA. *Glob Chang Biol* 17(2):886–897.
22. FLUXNET Synthesis Dataset (La Thuile 2007). Available at www.fluxdata.org/default.aspx. Accessed January 2014.
23. Heinsch FA, et al. (2003) *GPP and NPP (MOD17A2/A3) Products NASA MODIS Land Algorithm. MOD17 User's Guide*. Available at datamirror.csdb.cn/modis/resource/doc/MOD17_UsersGuide.pdf. Accessed November 2013.
24. Xiao X, Biradar C, Wang A, Sheldon S, Chen Y (2011) Recovery of vegetation canopy after severe fire in 2000 at the Black Hills National Forest, South Dakota, USA. *J Resour Ecol* 2(2):106–116.
25. Lentile LB, Smith FW, Shepperd WD (2005) Patch structure, fire-scar formation, and tree regeneration in a large mixed-severity fire in the South Dakota Black Hills, USA. *Can J For Res* 35(12):2875–2885.
26. Giorgi F, Lionello P (2008) Climate change projections for the Mediterranean region. *Glob Planet Change* 63(2-3):90–104.
27. Liu XJ, Ju XT, Zhang FS, Pan JR, Christie P (2003) Nitrogen dynamics and budgets in a winter wheat-maize cropping system in the North China Plain. *Field Crops Res* 83(2): 111–124.
28. Michaletz ST, Cheng D, Kerkhoff AJ, Enquist BJ (2014) Convergence of terrestrial plant production across global climate gradients. *Nature* 512(7512):39–43.
29. Schwartz MD, Ahas R, Aasa A (2006) Onset of spring starting earlier across the Northern Hemisphere. *Glob Chang Biol* 12(2):343–351.
30. Sacks WJ, Schimel DS, Monson RK (2007) Coupling between carbon cycling and climate in a high-elevation, subalpine forest: A model-data fusion analysis. *Oecologia* 151(1):54–68.
31. Hu J, Moore DJP, Burns SP, Monson RK (2010) Longer growing seasons lead to less carbon sequestration by a subalpine forest. *Glob Chang Biol* 16(2):771–783.
32. Buermann W, Bikash PR, Jung M, Burn DH, Reichstein M (2013) Earlier springs decrease peak summer productivity in North American boreal forests. *Environ Res Lett* 8(2):024027.
33. Jeong SJ, Ho CH, Kim BM, Feng S, Medvigy D (2013) Non-linear response of vegetation to coherent warming over northern high latitudes. *Remote Sens Lett* 4(2): 123–130.
34. Piao S, et al. (2013) Evaluation of terrestrial carbon cycle models for their response to climate variability and to CO_2 trends. *Glob Chang Biol* 19(7):2117–2132.
35. White MA, Thornton PE, Running SW (1997) A continental phenology model for monitoring vegetation responses to interannual climatic variability. *Global Biogeochem Cycles* 11(2):217–234.
36. Hodges T (1990) *Predicting Crop Phenology* (CRC, Boston).
37. Bonan GB, et al. (2011) Improving canopy processes in the Community Land Model version 4 (CLM4) using global flux fields empirically inferred from FLUXNET data. *J Geophys Res Biogeosci* 116(G2):G02014.
38. Xu L, Baldocchi DD (2003) Seasonal trends in photosynthetic parameters and stomatal conductance of blue oak (Quercus douglasii) under prolonged summer drought and high temperature. *Tree Physiol* 23(13):865–877.
39. Kattge J, Knorr W, Raddatz T, Wirth C (2008) Quantifying photosynthetic capacity and its relationship to leaf nitrogen content for global-scale terrestrial biosphere models. *Glob Change Biol* 15(4):976–991.
40. Dierenbach J, Badeck FW, Schaber J (2013) The plant phenological online database (PPODB): An online database for long-term phenological data. *Int J Biometeorol* 57(5):805–812.
41. Wolkovich EM, et al. (2012) Warming experiments underpredict plant phenological responses to climate change. *Nature* 485(7399):494–497.
42. Zhang X, et al. (2003) Monitoring vegetation phenology using MODIS. *Remote Sens Environ* 84(3):471–475.
43. Jones MO, Jones LA, Kimball JS, McDonald KC (2011) Satellite passive microwave remote sensing for monitoring global land surface phenology. *Remote Sens Environ* 115(4):1102–1114.
44. Richardson AD, et al. (2007) Use of digital webcam images to track spring green-up in a deciduous broadleaf forest. *Oecologia* 152(2):323–334.
45. Keenan TF, et al. (2014) Tracking forest phenology and seasonal physiology using digital repeat photography: A critical assessment. *Ecol Appl* 24(6):1478–1489.
46. Zhang Y, et al. (2014) Estimation of vegetation photosynthetic capacity from space-based measurements of chlorophyll fluorescence for terrestrial biosphere models. *Glob Chang Biol* 20(12):3727–3742.
47. Joiner J, et al. (2013) Global monitoring of terrestrial chlorophyll fluorescence from moderate spectral resolution near-infrared satellite measurements: Methodology, simulations, and application to GOME-2. *Atmos Meas Tech Discuss* 6(2):3883–3930.
48. Zhu Z, et al. (2013) Global data sets of vegetation leaf area index (LAI) 3g and Fraction of Photosynthetically Active Radiation (FPAR) 3g derived from Global Inventory Modeling and Mapping Studies (GIMMS) Normalized Difference Vegetation Index (NDVI3g) for the period 1981 to 2011. *Remote Sens (Basel)* 5(2):927–948.
49. Luo YQ, et al. (2012) A framework for benchmarking land models. *Biogeosciences* 9(10):3857–3874.
50. Guanter L, et al. (2014) Global and time-resolved monitoring of crop photosynthesis with chlorophyll fluorescence. *Proc Natl Acad Sci USA* 111(14):E1327–E1333.
51. Koster R, Walker G, Collatz G, Thornton P (2014) Hydroclimatic controls on the means and variability of vegetation phenology and carbon uptake. *J Clim* 27:5632–5652.
52. Heinsch FA, et al. (2006) Evaluation of remote sensing based terrestrial productivity from MODIS using regional tower eddy flux network observations. *IEEE Trans Geosci Remote Sens* 44(7):1908–1925.
53. Gu L, et al. (2003) *Phenology of Vegetation Photosynthesis. Phenology: An Integrative Environmental Science* (Springer, New York), pp 467–485.
54. Gu L, et al. (2009) *Characterizing the Seasonal Dynamics of Plant Community Photosynthesis Across a Range of Vegetation Types. Phenology of Ecosystem Processes* (Springer, New York), pp 35–58.
55. Eklundh L, Jönsson P (2012) *Timesat 3.1 Software Manual*.

Supplementary Information (SI) Appendix for

Joint Control of Terrestrial Gross Primary Productivity by Plant Phenology and Physiology

Jianyang Xia[1†*], Shuli Niu[2†*], Philippe Ciais[3], Ivan Janssens[4], Jiquan Chen[5], Christof Ammann[6], Altaf Arain[7], Peter D. Blanken[8], Alessandro Cescatti[9], Damien Bonal[10], Nina Buchmann[11], Peter S. Curtis[12], Shiping Chen[13], Jinwei Dong[1], Lawrence B. Flanagan[14], Christian Frankenberg[15], Teodoro Georgiadis[16], Christopher M. Gough[17], Dafeng Hui[18], Gerard Kiely[20], Jianwei Li[1,18], Magnus Lund[20], Vincenzo Magliulo[21], Barbara Marcolla[22], Lutz Merbold[11], Leonardo Montagnani[23,24], Eddy Moors[25], Jørgen E. Olesen[26], Shilong Piao[27], Antonio Raschi[28], Olivier Roupsard[29,30], Andrew E. Suyker[31], Marek Urbaniak[32], Francesco P. Vaccari[28], Andrej Varlagin[33], Timo Vesala[34,35], Matthew Wilkinson[36], Ensheng Weng[37], Georg Wohlfahrt[38,39], Liming Yan[40], Yiqi Luo[1†*],

[1]Department of Microbiology and Plant Biology, University of Oklahoma, OK, USA;

[2]Synthesis Research Center of Chinese Ecosystem Research Network, Key Laboratory of Ecosystem Network Observation and Modeling, Institute of Geographic Sciences and Natural Resources Research, Chinese Academy of Sciences, Beijing, China;

[3]Laboratoire des Sciences du Climat et de 1'Environnement, CEA CNRS UVSQ, 91191 Gif sur Yvette, France;

[4]Department of Biology, University of Antwerpen, Universiteitsplein 1, 2610Wilrijk, Belgium;

[5]Center for Global Change and Earth Observations (CGCEO), and Department of Geography, Michigan State University, MI, USA;

[6]Federal Research Station Agroscope, Climate and Air Pollution Group, Zuerich, Switzerland;

[7]School of Geography and Earth Sciences, McMaster University, Hamilton, ON, Canada L8S 4K1;

[8]Department of Geography, University of Colorado at Boulder, 260 UCB, Boulder, CO, USA;

[9]European Commission, Joint Research Center, Institute for Environment and Sustainability, Ispra, Italy;

[10]INRA, UMR 1137 INRA-Université de Lorraine, 54280 Champenoux, France;

[11]Institute of Agricultural Sciences, ETH Zurich, 8092 Zurich, Switzerland

[12]Department of Evolution, Ecology & Organismal Biology, The Ohio State University, Columbus, OH, USA;

[13]State Key Laboratory of Vegetation and Environmental Change, Institute of Botany, Chinese Academy of Sciences, No.20 Nanxincun, Xiangshan, Beijing 100093, China;

[14]Department of Biological Sciences, University of Lethbridge, Lethbridge, Alberta, TIK 3M4, Canada;

[15]Jet Propulsion Laboratory, M/S 183-601, 4800 Oak Grove Drive, Pasadena, CA, USA;

[16]IBIMET-CNR, Via P. Gobetti 101, 40129 Bologna, Italy;

[17]Department of Biology, Virginia Commonwealth University, Richmond, VA, USA;

[18]Department of Biological Sciences, Tennessee State University, TN, USA;

[19]Civil and Environmental Engineering Department, and Environmental Research Institute, University College Cork, Cork, Ireland;

[20]Department of Bioscience, Aarhus University, Frederiksborgvej 399, 4000, Roskilde, Denmark;

[21]CNR–ISAFOM, Institute for Mediterranean Agricultural and Forest Systems, National Research Council, via Patacca 85, 80040 Ercolano (Napoli), Italy;

[22]Sustainable Agro-ecosystems and Bioresources Department, Fondazione Edmund Mach, Via E. Mach, 1 38010 S. Michele all'Adige (TN), Italy;

[23]Servizi Forestali, Provincia Autonoma di Bolzano, 39100 Bolzano, Italy;

[24]Faculty of Science and Technology, Free University of Bolzano, Piazza Universita 5, 39100 Bolzano, Italy;

[25]ESS-CC, Alterra, Wageningen UR, PO Box 47, 6700 AA Wageningen, The Netherlands;

[26]Department of Agroecology, Aarhus University, Blichers Allé 20, DK-8830 Tjele, Denmark;

[27]Department of Ecology, College of Urban and Environmental Sciences, Peking University, Beijing 100871, China;

[28]IBIMET-CNR, Via G. Caproni 8 50145 Firenze, Italy;

[29]CIRAD, UMR Eco&Sols (Ecologie Fonctionnelle & Biogéochimie des Sols et des Agro-écosystèmes), 34060 Montpellier, France;

[30]CATIE (Tropical Agricultural Centre for Research and High Education), 7170 Turrialba, Costa Rica;

[31]Hardin Hall, 3310 Holdrege Street, University of Nebraska-Lincoln, Lincon, Nebraska, USA;

[32]Department of Meteorology, Poznan University of Life Sciences, Piatkowska 94, 60649 Poznan, Poland;

[33]A. N. Severtsov Institute of Ecology and Evolution, Russian Academy of Sciences, Leninsky pr.33, Moscow, 119071, Russia;

[34]Department of Physics, P.O. Box 48, FIN-00014 University of Helsinki, Finland;

[35]Department of Forest Sciences, P.O.Box 27, FIN-00014, University of Helsinki, Finland;
[36]Centre for Sustainable Forestry & Climate Change, Forest Research, Farnham, UK;
[37]Department of Ecology and Evolutionary Biology, Princeton University, NJ, USA;
[38]Institute of Ecology, University of Innsbruck, Sternwartestr. 15, 6020 Innsbruck, Austria;
[39]European Academy of Bolzano, Drususallee 1, 39100 Bolzano, Italy;
[40]School of Life Sciences, Fudan University, 220 Handan Road, Shanghai, 200433, China

[†]These authors contributed equally to this work.

*To whom correspondence should be addressed. jxia@ou.edu, sniu@igsnrr.ac.cn or yluo@ou.edu

56 pages (including cover page)

S1 Materials and Methods

S1.1 Data

S1.1.1 The FLUXNET La Thuile Database

The ecosystem-level GPP were estimated by the eddy covariance technique, a key method to measure the net ecosystem-atmosphere exchange of CO_2(1). The eddy covariance technique provides a useful tool to study the seasonal dynamics of plant-community level photosynthesis(2). We used data of gross primary productivity (GPP; positive GPP means CO_2 uptake) from 213 FLUXNET sites from the La Thuile Database (www.fluxdata.org, Table S1) in our analyses. The database was a combination of measurements from the networks Ameriflux, CarboEurope and Fluxnet-Canada, and covers the time period of 1993–2006. Data of each site-year in the database was filtered according to the methods and criteria in Reichstein *et al*.(3) and Papale *et al*.(4). Since the GPP data are not directly measured, they include some inevitable uncertainties. The sources of those uncertainties have been widely discussed by Beer *et al*.(5), Moncrieff et al.(6), Papale *et al*.(4), Moffat *et al*.(7) and Desai *et al*.(8). Since there is no phenological information in diurnal variations of CO_2 fixation, we used daily GPP in this study. There are some negative values for daily GPP in some site years. Only site years with more than 300 daily estimates were chosen from the database.

S1.1.2 MODIS GPP

We used the data of gross primary productivity (GPP) from the Moderate Resolution Imaging Spectroradiometer (MODIS) aboard NASA's Terra satellites (MOD17A2 GPP(9)) for North America (7.05–79.95°N, 58.55–98.85°W) during 2000-2010 in our analyses. The data set was generated by the Numerical Terradynamic Simulation Group (NTSG)/University of Montana's (UMT) as Version-55 and available from the LP DAAC(10, 11). The algorithm of MODIS GPP is described in Running *et al*.(12) and Zhao *et al*.(10). This product has considered the cloud-contamination issue while the NASA's MOD17 products (i.e., Version-5 GPP) did not. Thus, this product can avoid the underestimation in the MOD17A2-V5 products (13). The accuracy of this product has been assessed by using independent measurements made in a systematic and statistically robust way and feasible for the application of scientific community. We downloaded the data and mosaicked and re-projected the data by using the MODIS Reprojection Tool. The mosaicked images were resampled into 0.1 ° × 0.1 °by using the nearest neighbor algorithm.

S1.2 Characteristics of annual GPP curve: definitions

In most terrestrial ecosystems, the daily GPP throughout the whole year follows a bell-shaped curve, which can be represented by the idealized solid black line in the following figure:

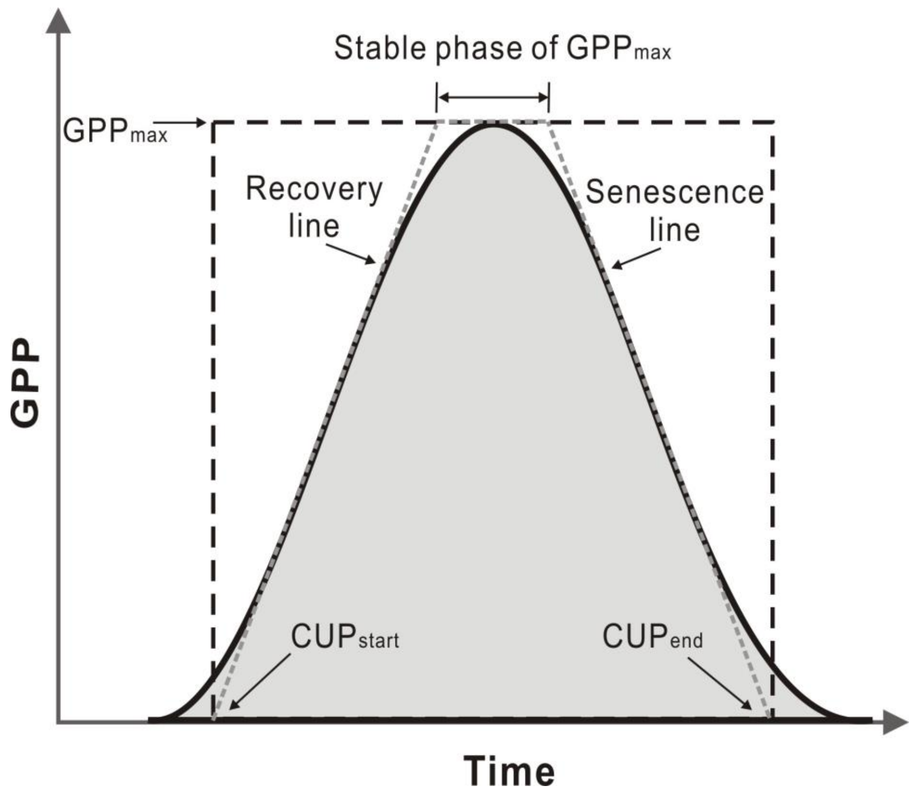

Supplementary Fig. S1.2.1. Ideal curve of seasonal GPP in terrestrial ecosystem.

The shape of the above unimodal curve (Fig. S1.2.1) is determined by five consecutive phases, which are described by Gu *et al*.(14):

Phase 1. Transition stage from non-growing to growing season, with a slowly increasing GPP.

Phase 2. Recover stage with rapidly increasing GPP.

Phase 3. Stable stage in the middle of the growing season, during which the plant community keeps its maximal GPP relatively stable.

Phase 4. Senescence stage with rapidly declining GPP.

Phase 5. Transition stage from growing no non-growing season, with a slowly declining GPP.

The above phases of seasonal cycle of GPP include a combination of characteristics in sequence as follows:

1. ***CUP_{start}***. The start day of CO_2 uptake period during a year.
2. ***Peak recovery rate of GPP***. In non-evergreen ecosystems, when plant community starts CO_2 fixation from the atmosphere in spring (or in newly started crops), the daily GPP rate recovers from 0 and gradually approaches its peak. The peak recovery rate of GPP can be obtained from the slope of the recovery line in Fig. S1.2.1.
3. ***GPP_{max}***. The maximal daily GPP during the growing season.
4. ***Stable phase of GPP_{max}***. The stable phase in which plant community keeps maximal GPP.
5. ***Peak senescence rate of GPP***. It represents the peak rate of GPP reduction during late growing season in non-evergreen ecosystems, and can be obtained from the slope of the senescence line in Fig. S1.2.1.
6. ***CUP_{end}***. The end day of CO_2 uptake period during a year.

We define the CUP (carbon uptake period) as the number of days per year with GPP > 0. As a consequence, the CUP of an ecosystem can be calculated from CUP_{start} and CUP_{end}. CUP represents the duration of vegetation photosynthetic phenology, which is one of the functional aspects of plant phenology(14).

S1.3 Representation of the seasonal cycle of GPP

The seasonal cycle of daily GPP varies over time and across ecosystems and regions. In general, GPP seasonality in terrestrial ecosystems can be categorized into four types, including (1) one-peak during the summer-autumn growing seasons, (2) one-peak during the winter-spring seasons, (3) multiple peaks during the whole year, and (4) low seasonality such as the tropical ecosystems. Since no single function can describe the diverse GPP dynamics across the globe, we use different strategies to obtain the characteristics of annual GPP dynamics (S1.2) for each of four types of GPP seasonality above. First, we judged whether the site-year or grid cell is evergreen or not, by counting the number of days with larger daily GPP than a given value. In a second step, the number of seasons in the rest site-years or land grid cells was determined by a model function (equation 6). For those site-years and grid cells with one season, we fitted a 5-parameter Weibull function to the data from that year. For those site-years or land grid cells with more than one season, we fitted the Weibull function to each season. More details for the analyses and determinations of CUP and GPP_{max} are provided as follows:

S1.3.1. Low seasonality such as the tropical ecosystems

In some ecosystems, especially in tropical regions, the seasonality is low, and their CUP usually approaches 365 days (or 366 days in leap years). For example, as shown in Fig. S1.3.1, the dynamic of daily GPP in the sites of BR-Sa1, US-SP3 and BR-Cax does not include obvious recovery or senescence stages in a single year.

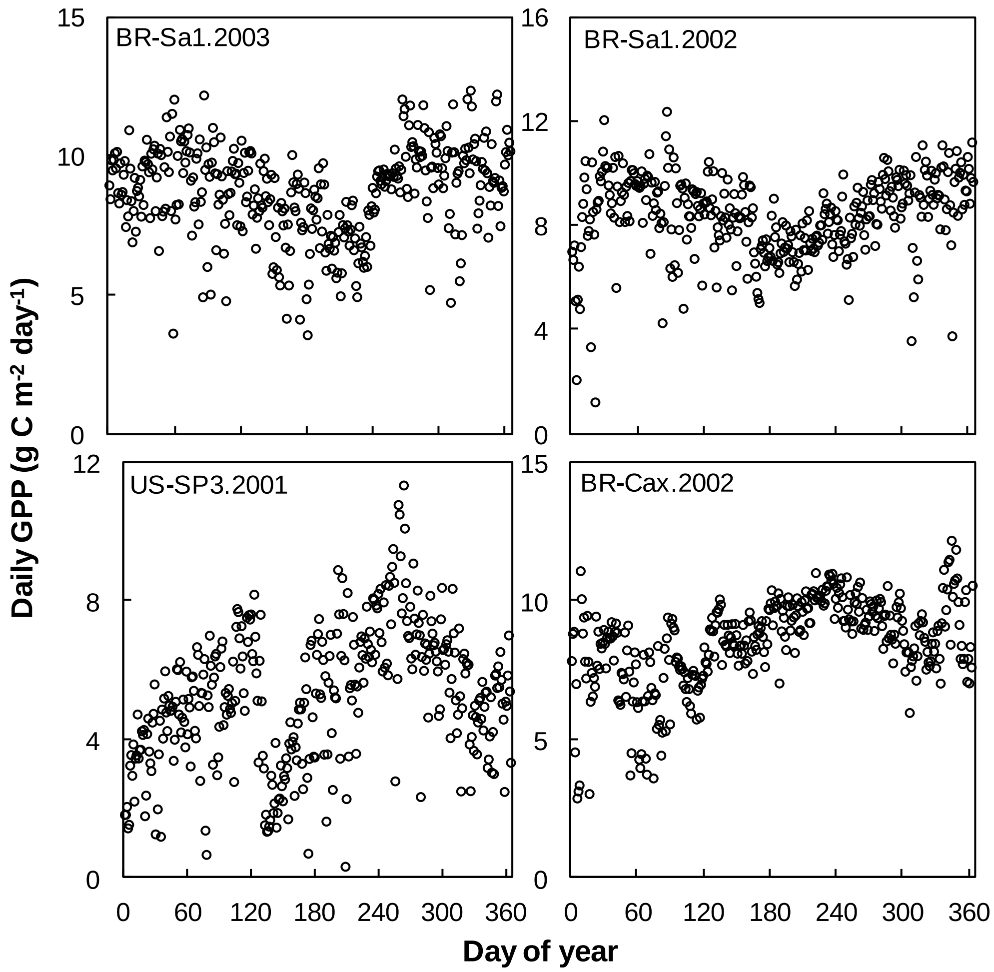

Supplementary Fig. S1.3.1. Examples of evergreen site-year with low seasonality of daily GPP . The details of the sites BR-Sa1, US-SP3 and BR-Cax can be found in Table S1.

In this study, we first judge if the site-year or grid cell is evergreen or not, by counting the number of days with larger daily GPP than a given value. Here, if there are more than 360 days with daily GPP > 1 g C m^{-2} day^{-1} in a site-year, the site-year is defined as evergreen with CUP = 365 (366 for leap years). For the MODIS GPP with the 8-day interval, we obtained daily GPP for the whole year through the linear trend between each two adjacent observations:

$$GPP(i) = GPP(i) + (i-1)\frac{GPP(i+1) - GPP(i)}{8} \qquad (1)$$

where i is the ith day of a given year.

To get the GPP_{max} in the whole year, we first smoothed the GPP time series using a simple moving average method, which replaces the GPP in ith day of a given year (GPP_i, i = 1, 2, ..., N) by a linear combination of nearby values in a window(15):

$$\sum_{j=-n}^{n} c_j GPP_{i+j} \qquad (2)$$

where c_j represents the weighted factor and equals 1/(2n+1). The data of GPP_i is replaced by the values in the window calculated by the equation (2). In this study, we choose n = 3 to smooth the observed daily GPP. Then the maximal daily GPP was chosen as the GPP_{max} in that year.

S1.3.2. Multiple peaks during the whole year

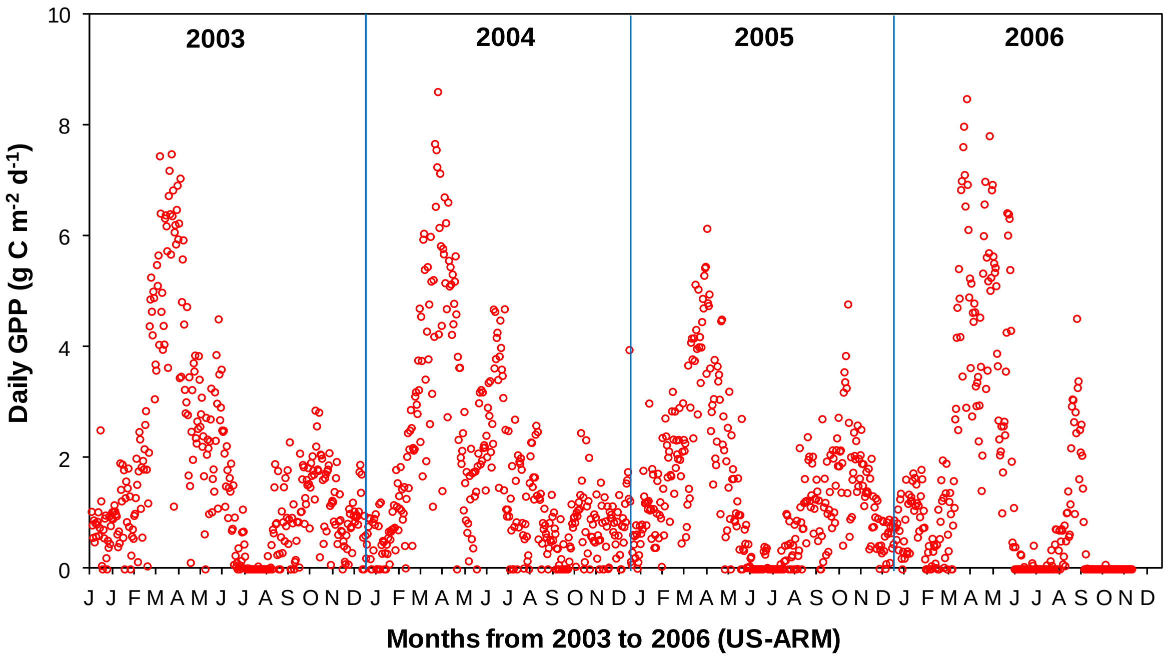

Supplementary Fig. S1.3.2. Observed daily GPP from 2003 to 2006 in the flux site of US-Arm (please see its details in Table S1). This figure shows there are mainly two peaks in this ecosystem, with one around April and the other in October. Note that the negative values from the database have been replaced by 0, and the observations after 324*th* day in 2004 were missing in the original database.

In some ecosystems, e.g., the Mediterranean-climate regions(16), some regions in the Great Plains in the US(17) and multiple yield cropping systems(18), there are more than one vegetation peak during one year. As shown in Fig. S1.3.2, there are two peaks of daily GPP in each year in the flux site of US-Arm, with one peak occurring around April and the other in October. The multiple GPP cycles were analyzed separately with the Weibull function (see S1.3.3 and the equation 7) and their results were weighted to describe the CUP and GPP_{max} in the whole year.

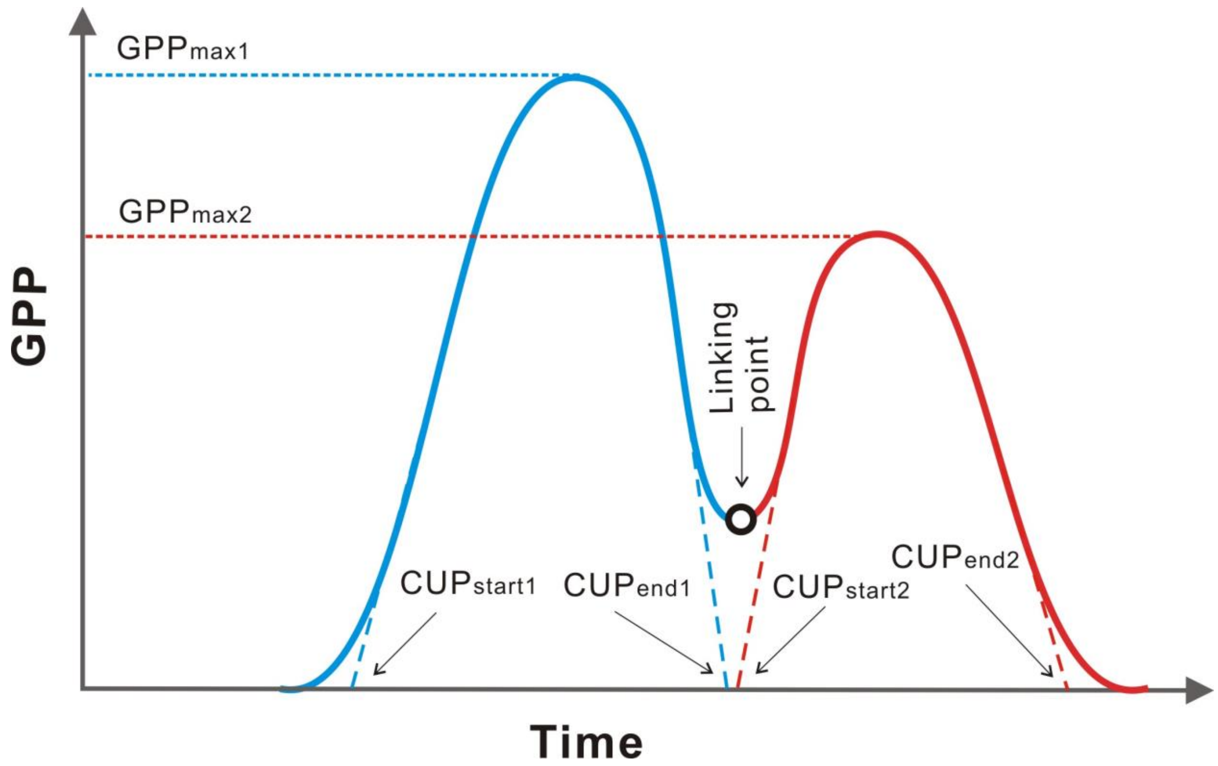

Supplementary Fig. S1.3.3. Idealized curve of GPP dynamic and its characteristics in sites with two peaks in a single year. The blue and red curve respectively represent the first and second cycle of GPP in this year.

Since sometime the two GPP cycles overlap (as shown by Fig. S1.3.3), the weighted integration of CUP from the two GPP cycles within one year was conducted as:

$$CUP = \begin{cases} CUP_1 + CUP_2 & if\ no\ overlap\ between\ the\ two\ GPP\ cycles \\ CUP_{end2} - CUP_{start1} & if\ there\ is\ overlap\ between\ the\ two\ GPP\ cycles \end{cases} \quad (3)$$

where CUP_1 and CUP_2 are the CO_2 uptake period in the first and second GPP cycle, respectively. CUP_{srart1} is the initiation day of CUP for the first GPP cycle, and CUP_{end2} is the termination day of CUP for the second GPP cycle. The weighted integration of GPP_{max} is more complex because it depends on not only whether but also when the two GPP cycles overlap. In this study, if there is no overlap between the two GPP cycles, the yearly GPP_{max} is weighted as:

$$GPP_{max} = (GPP_{max1}CUP_1 + GPP_{max2}CUP_2)/(CUP_1 + CUP_2) \quad (4)$$

If there is overlap between the two GPP cycles, then the yearly GPP_{max} cannot be directly weighted as in equation 7. For these sites, we first find out the linking day (D_{link}) between the two GPP cycles (see the black circle in Fig. S1.3.3). Then, the weighted GPP_{max} was calculated as:

$$GPP_{max} = \frac{GPP_{max1}(D_{link} - CUP_{start1}) + GPP_{max2}(CUP_{end2} - D_{link})}{CUP_1 + CUP_2} \quad (5)$$

The same strategy as the above equations has been used if there are more than two growing seasons. Thus, one of the key steps in analyzing the GPP data in sites with multiple peaks in a single year is to determine the number of seasons. However, the GPP observations often have high-level noise (as shown by Fig. S1.3.2, S1.3.4 and S1.3.5), making it difficult to determine the number of seasons with only one year of data(19). In this study, we reduced the risk for erroneous determination of season number by triplicating the yearly GPP dynamic (see the gray circles in Fig. S1.3.5). Then, we followed the method that is used in the TIMESAT software(19), by fitting the daily GPP data (t_i, GPP_i), i = 1, 2, ..., n for all 3 years (as shown in Fig. S1.3.5) to the following function:

$$f(t) = c_1 + c_2 \sin(\omega t) + c_3 \cos(\omega t) + c_4 \sin(2\omega t) + c_4 \cos(2\omega t) \qquad (6)$$

where $\omega = 6\pi/n$. C_1 determines the base level, while $c_2 \sin(\omega t) + c_3 \cos(\omega t)$ and $c_4 \sin(2\omega t) + c_4 \cos(2\omega t)$ determine the number of seasons as one and two, respectively. During the fitting, a primary maximum is always found and a secondary maximum may be found. As suggested by TIMESAT(19), the amplitude ratio between the secondary maximum and the primary maximum can be used as an index to determine the number of vegetation seasons. That is, if the ratio is below a given threshold, the ecosystem has one season during the year. In this study, we set the ratio between the secondary maximum and the primary maximum as 0.25. For example, as shown in Fig. S1.3.5, the fitted secondary and primary maximum in 2000 in the grid of N37.75^o, W101.05^o are 1.69 and 2.68 g C m^{-2} d^{-1}, respectively, and the ratio between them is 0.63. It means there are two vegetation seasons in this grid cell in 2000 (Fig. S1.3.5).

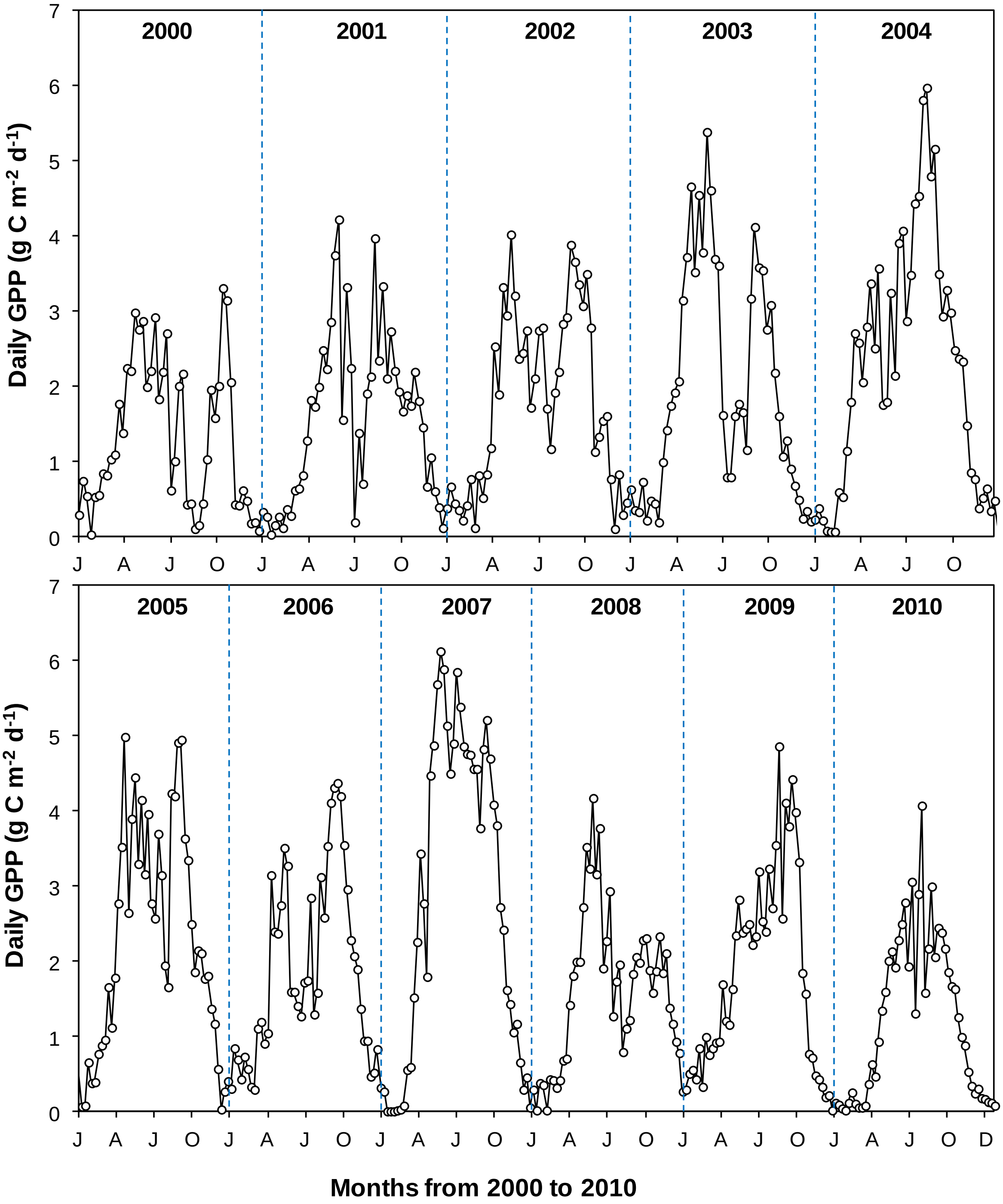

Supplementary Fig. S1.3.4. MODIS daily GPP from 2000 to 2010 in the grid cell of N37.75º, W101.05º. The data in the original database were in 8-day interval.

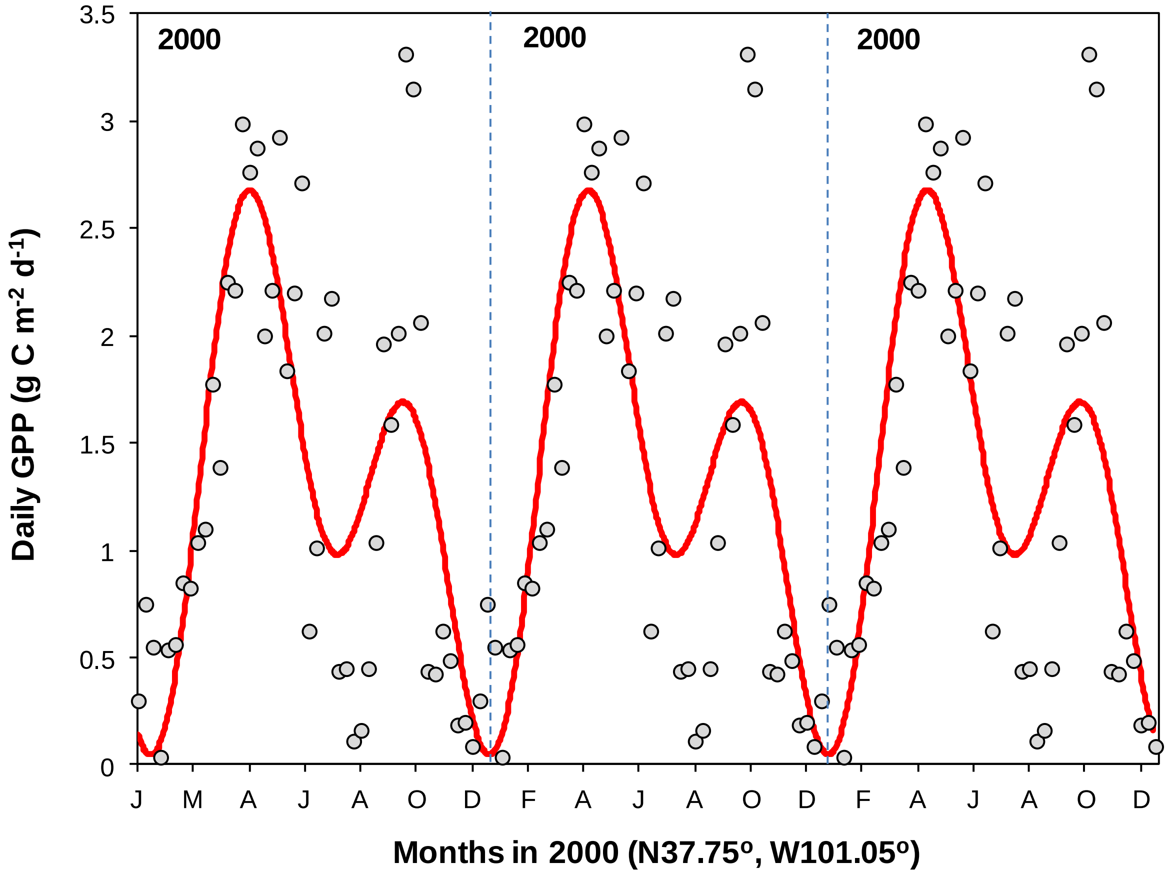

Supplementary Fig. S1.3.5. Triplicate of MODIS GPP in 2000 in the grid cell of N37.75°, W101.05° . The gray circles are the 8-day interval GPP values from the original database. The red line is the fitted GPP dynamic with the equation (6).

S1.3.3. One-peak during the summer-autumn growing seasons

In many terrestrial ecosystems, vegetation season peaks around the middle of growing season, and the seasonal cycles of daily GPP can be represented by the idealized curve in Fig. S1.2.1. In order to obtain all the characteristics (see S1.2) from both FLUXNET and MODIS-based GPP, we fitted a 5-parameter Weibull function to the data from each year. The Weibull function is given as:

$$P(t) = \begin{cases} y0 + a\left(\frac{c-1}{c}\right)^{\frac{1-c}{c}} (\left|\frac{t-x0}{b} + \left(\frac{c-1}{c}\right)^{\frac{1}{c}}\right|^{c-1} e^{\left(-\left|\frac{t-x0}{b}+\left(\frac{c-1}{c}\right)^{\frac{1}{c}}\right|^{c} + \frac{c-1}{c}\right)} & if\ \ t \le x0 - b\frac{c-1}{c} \\ y0 & if\ t > \ x0 - b\frac{c-1}{c} \end{cases} \quad (7)$$

where *t* represents the number of days in each year, and *P(t)* is the corresponding daily mean GPP (g C m^{-2} day^{-1}); *x*0, *y*0, *a*, *b*, and *c* are empirical parameters to be estimated. As shown below, this function is flexible and fits one-peak seasonal GPP well in contrasting biomes and years. Similar Weibull functions have been successfully applied to fit seasonal dynamics of plant community photosynthesis. For example, Gu *et al*.(2) used a Weibull function to fit the seasonal cycle of plant community photosynthesis separately by dividing the growing season in its middle peak. Recently, Gu *et al*.(14) developed a new 9-parameter Weibull function capable of capturing both recovery and senescence parts of the growing season. The Weibull function used in this study captures both recovery and senescence parts of GPP dynamics, and consists of fewer empirical parameters (equation 7; 5 parameters). It has been used as a default function to fit one-peak time-series data in the Sigmaplot (Systat Software, Inc, San Jose, CA, USA).

The fitting of data to the equation 7 was conducted in the R software (version 2.13.0; http://www.R-project.org). The details of the model fitting with nonlinear regression can be found in the section S1.4. After the curve fitting, we can obtain the fitted daily GPP in a given year. The maximal daily GPP (GPP_{max}) is obtained as:

$$GPP_{max} = \max\ \{P(t)\} \quad (8)$$

where *P(t)* (*t* = 1, 2, ... , n) is the daily GPP in the *t*th day, and n is 365 for regular years and 366 for leap years. The CO_2 uptake period (CUP) is determined by the initiation (CUP_{start}) and termination (CUP_{end}) days of CUP as:

$$CUP = CUP_{end} - CUP_{start} \quad (9)$$

Since plant community photosynthesis usually fluctuates at the start and end of CUP (as shown in the Fig. S1.3.6), it is difficult to determine the days in which the ecosystem starts or stops the CO_2 uptake. In this study, we calculated the CUP_{start} as the intersection between the recovery line (see the left red dashed line in Fig. S1.3.6) and the time (day of year) axis. Similarly, the CUP_{end} was obtained by the intersection between the senescence line (see the right red dashed line in Fig. S1.3.6) and the time axis. Previous studies (2, 14) have found this approximation can capture the initiation and termination days of plant community photosynthesis in most terrestrial ecosystems. Thus, in order to calculate the CUP_{start} and CUP_{end}, we need to first get the recovery and senescence lines.

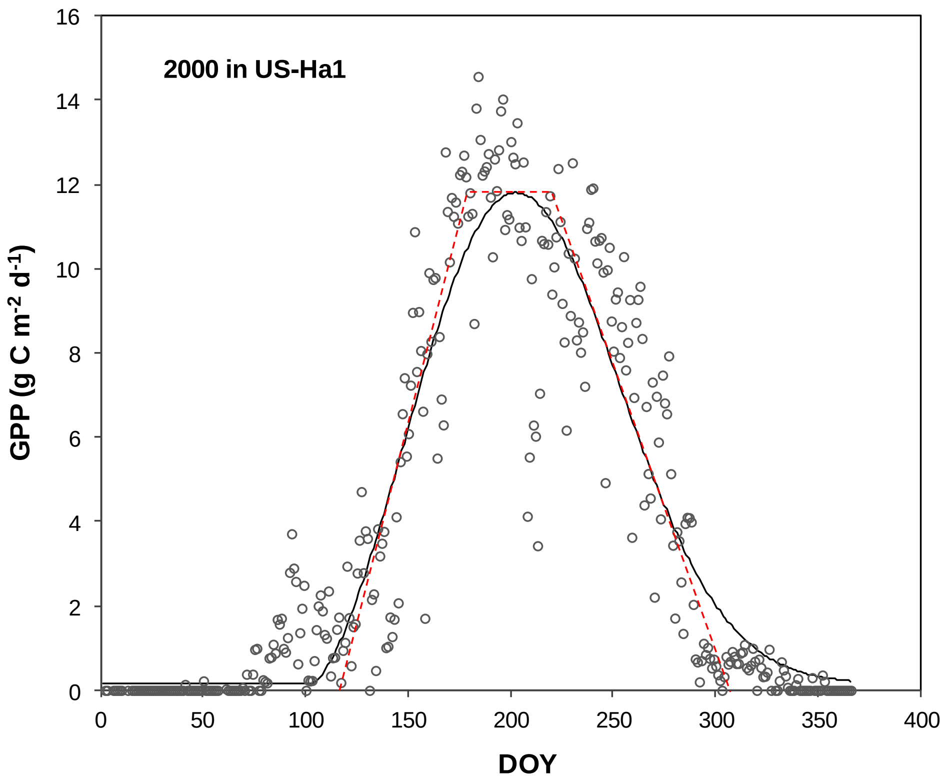

Supplementary Fig. S1.3.6. An example of fitting the equation 7 to GPP observations from US-Ha1 in 2000. The black solid line is the fitted curve. The red dashed lines represent recovery, stable phase of GPP_{max}, and senescence line in sequence.

The recovery and senescence lines represent the maximum and minimum in the growth rate of daily GPP, respectively. Here, we use a moving linear regression approach to seek the day in which the growth rate of daily GPP reaches maximum and minimum. The linear model used in estimating the growth rate of daily GPP is:

$$P(t) = \beta t + \beta_0 \quad (10)$$

where β is the theoretical slope representing the growth rate of daily GPP, and β_0 is the theoretical y-intercept. We conducted the linear regression analysis for day *t* by using the data from day *t* - 3 to *t* + 3 (3 < *t* < *m*-3; *m* is 365 in regular years and 366 in leap years). The slope β in each day can be estimated by:

$$\hat{\beta}(t) = \frac{7\sum_{i=t-3}^{t+3} iP(i) - \sum_{i=t-3}^{t+3} i \sum_{i=t-3}^{t+3} P(i)}{7\sum_{i=t-3}^{t+3} i^2 - (\sum_{i=t-3}^{t+3} i)^2} \quad (11)$$

The maximal (R_{max}) and minimal (R_{min}) change rate of daily GPP are obtained by:

$$R_{max} = \max\ \{\hat{\beta}(t)\} \quad (12)$$

$$R_{min} = \min\ \{\hat{\beta}(t)\} \quad (13)$$

The associated *t* with R_{max} and R_{min} are the days (t_{max} and t_{min}) in which maximal and minimal change rate of daily GPP occurred, respectively. Note that the value of R_{max} is positive and R_{min} is negative. Thus, the CUP_{start} and CUP_{end} can be calculated as:

$$CUP_{start} = t_{max} - \frac{P(t_{max})}{R_{max}} \quad (14)$$

$$CUP_{end} = t_{min} - \frac{P(t_{min})}{R_{min}} \quad (15)$$

Similarly, the stable phase of GPP_{max} (SP_{gppmax}) can be calculated as:

$$SP_{gppmax} = SP_{gppmax\_end} - SP_{gppmax\_start} \quad (16)$$

where SP_{gppmax_start} and SP_{gppmax_end} are the start and end days of SP_{gppmax}, and can be solved by:

$$SP_{gppmax\_start} = t_{max} + \frac{GPP_{max} - P(t_{max})}{R_{max}} \quad (17)$$

$$SP_{gppmax\_end} = t_{min} + \frac{GPP_{max} - P(t_{min})}{R_{min}} \quad (18)$$

The main aim of this study is to examine the dependence of annual GPP on CUP and GPP_{max}. Such dependence can be represented by the ratio (α) between annual GPP and the product of CUP and GPP_{max} as:

$$\alpha = \frac{Annual\ GPP}{CUP \times GPP_{max}} \quad (19)$$

where the annual GPP is the sum of daily GPP from the original observed data.

S1.3.4. One-peak during the winter-spring seasons

In some ecosystems, the peak of daily GPP does not occur during summer-autumn seasons, but in winter or spring. For example, in some (semi-) arid regions with the Mediterranean climate, plant photosynthesis is high in mild/wet winter and spring and is low in hot/dry summer(20). As shown by Fig. S1.3.7, the daily GPP recovers in autumn, peaks in spring, and senesces in summer in the Yatir forest (IL-Yat; 31 °20'N, 35 °03'E), which is located between three distinct landscapes, including Hebron mountains, Beersheba plateau/Negev desert, and the Judean Desert and the Dead Sea Valley(21). For these sites and grids, a direct application of the equation 7 cannot capture the CUP. In the IL-Yat case, the

CUP will be underestimated because the CO_2 uptake period during September-December is ignored (Fig. S1.3.7).

For those sites and grids whose daily GPP peaks during spring or winter seasons, we obtained the entire growing season by duplicating the GPP dynamics (as shown by Fig. S1.3.8). As shown in Fig. S1.3.8, with the duplicate of daily GPP in 2001, an adjusted GPP dynamic can be obtained from August to July (as shown in red circles in Fig. S1.3.8). A key issue in this method is to determine the start and end day of the adjusted GPP dynamic. Since the FLUXNET GPP data are usually fluctuating with time, we determined the start and end day of the adjusted GPP dynamic by two steps:

(1) We first smooth the observed data by using a moving average method as equation 2 with n=3.

(2) Based on the smoothed curve in the step (1), we determined the start point of the adjusted GPP dynamic as the day (D_{start}) with the minimum GPP throughout the year, and the end day (D_{end}) according to the number of days in that year.

In the MODIS GPP product, the GPP dynamic with 8-day intervals is comparably smoother, so we only applied step (2) to get the adjusted GPP dynamic. The above adjusted GPP dynamic was then used for the analysis of CUP and GPP_{max} as the regular one-peak GPP curve in the Fig. S1.3.6. Although this method with adjusted GPP dynamic may generate some errors, it can provide a good estimation of CUP and GPP_{max} for those regions in where the single peak of daily GPP occurs in winter or spring seasons.

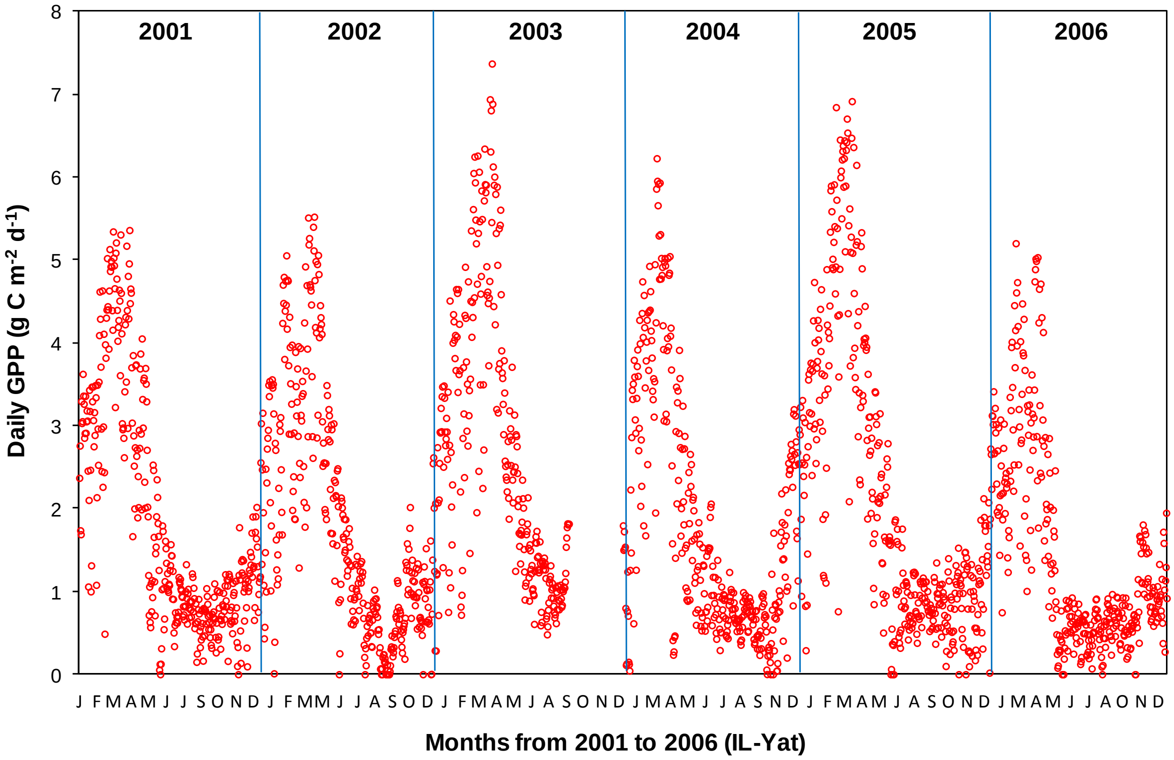

Supplementary Fig. S1.3.7. Observed daily GPP from 2001 to 2006 at the flux site of IL-Yat (please see its details in Table S1). Note that the negative values from the database has been replaced by 0, and the observations in Oct-Dec, 2004 were missing in the original database.

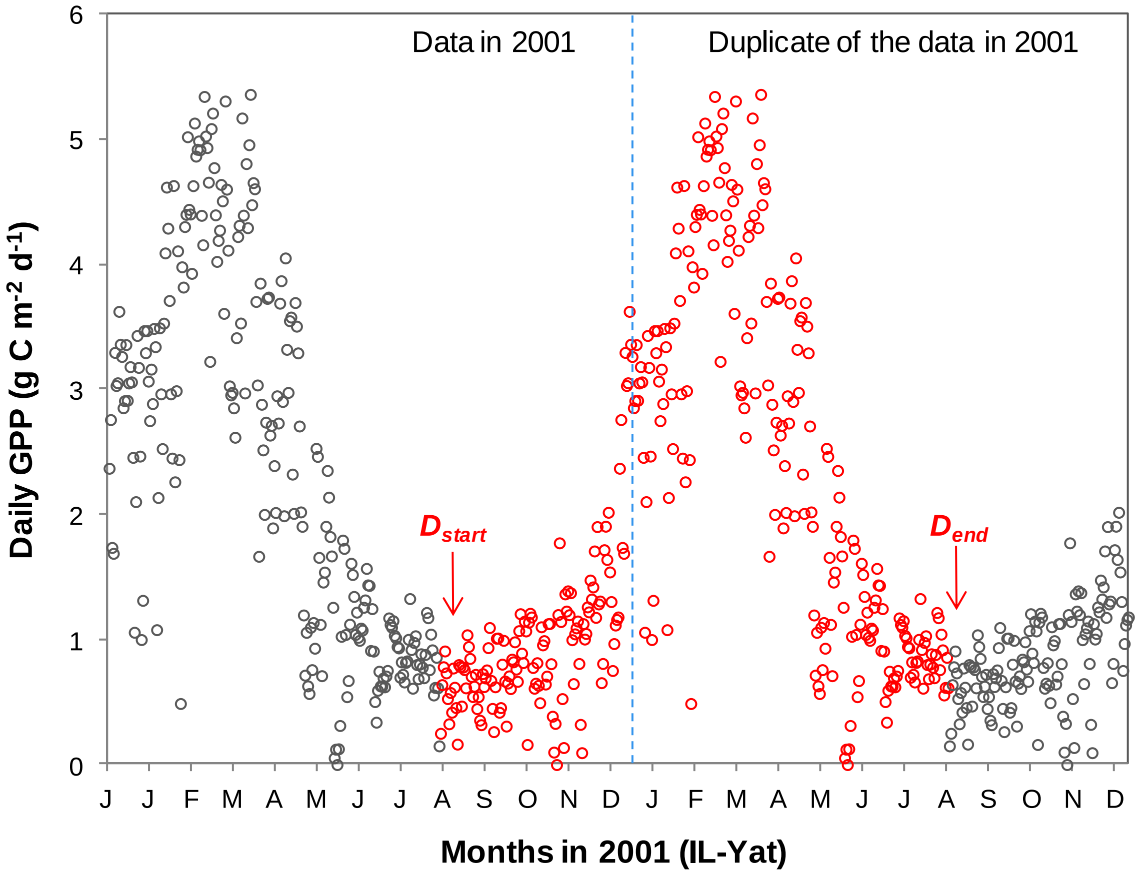

Supplementary Fig. S1.3.8. The figure shows how GPP data from those sites with winter-spring peaks were adjusted and analyzed in this study. The open circles on the left side of the blue dashed line are observed daily GPP in 2001 in IL-Yat site, and those on the right side of the blue dashed line are duplicated from the observed data in 2001. Then the red open circles represent the adjusted GPP dynamic and are used in the analysis of CUP and GPP_{max} in 2001 for IL-Yat. Note that the negative values from the database have been replaced by 0.

S1.4 Non-linear regression with R

As shown in both the equations 6 and 7, there are 5 unknown parameters determining the GPP dynamic against time in a given year. In this study, we used the general normal nonlinear regression model to fit the equations 6 and 7 to the observations. In general, the nonlinear regression model can be written as:

$$\mathrm{y}_i = f(X_i, \beta) + \varepsilon_i \qquad (21)$$

where y_i is the observed GPP in each year, f is the expectation function, and X_i is a vector of time (days in a single year). β is a vector including the 5 parameters in the equations 6 and 7, and ε_i is the error term for observation i. The error ε_i varies from year to year, and the errors are assumed to be normally distributed with mean 0 and constant variance: $\varepsilon_i \sim \mathrm{N}\ (0, \sigma^2)$.

The best estimates of the parameters (β) represent the best fit of the f function to the observations y_i. They can be obtained by minimization of the sum of squared residuals (S) with respect to β:

$$S(\beta) = \sum_{i=1}^{n} (y_i - f(X_i, \beta))^2 \qquad (22)$$

In each step, the Gauss-Newton method is used to determine the new parameters values based on the data, with the purpose to make the $S(\beta)$ as small as possible. More information about the nonlinear regression can be found in Bates and Watts (22) and Fox(23).

In this study, the non-linear regressions were performed with the model fitting function *nls*, which is located in the standard *nls* library in **R**. The parameter estimates are obtained from the non-linear model fitting, and then used for the analyses of GPP properties in S1.3.

S1.5 The performance of the Weibull function in capturing GPP dynamics in terrestrial ecosystem

Since GPP dynamics in many terrestrial ecosystems follow the single-peak curve like Fig. S1.3.6, it is important to make sure that equation 7 can capture GPP properties in contrasting biomes. Before we applied the equation 7 to all flux sites and grid cells, we first examined its performance in the years with contrasting climate conditions at long-term flux sites. The results show that the equation can well capture all years of GPP dynamics from those long-term sites. As shown by Fig. S1.5.1, the simulated GPP curve fits observations from years with highest, normal, and lowest values in each site well. It indicates the Weibull function used in this study has the ability to capture GPP dynamics and the associated properties in contrasting biomes and climate conditions.

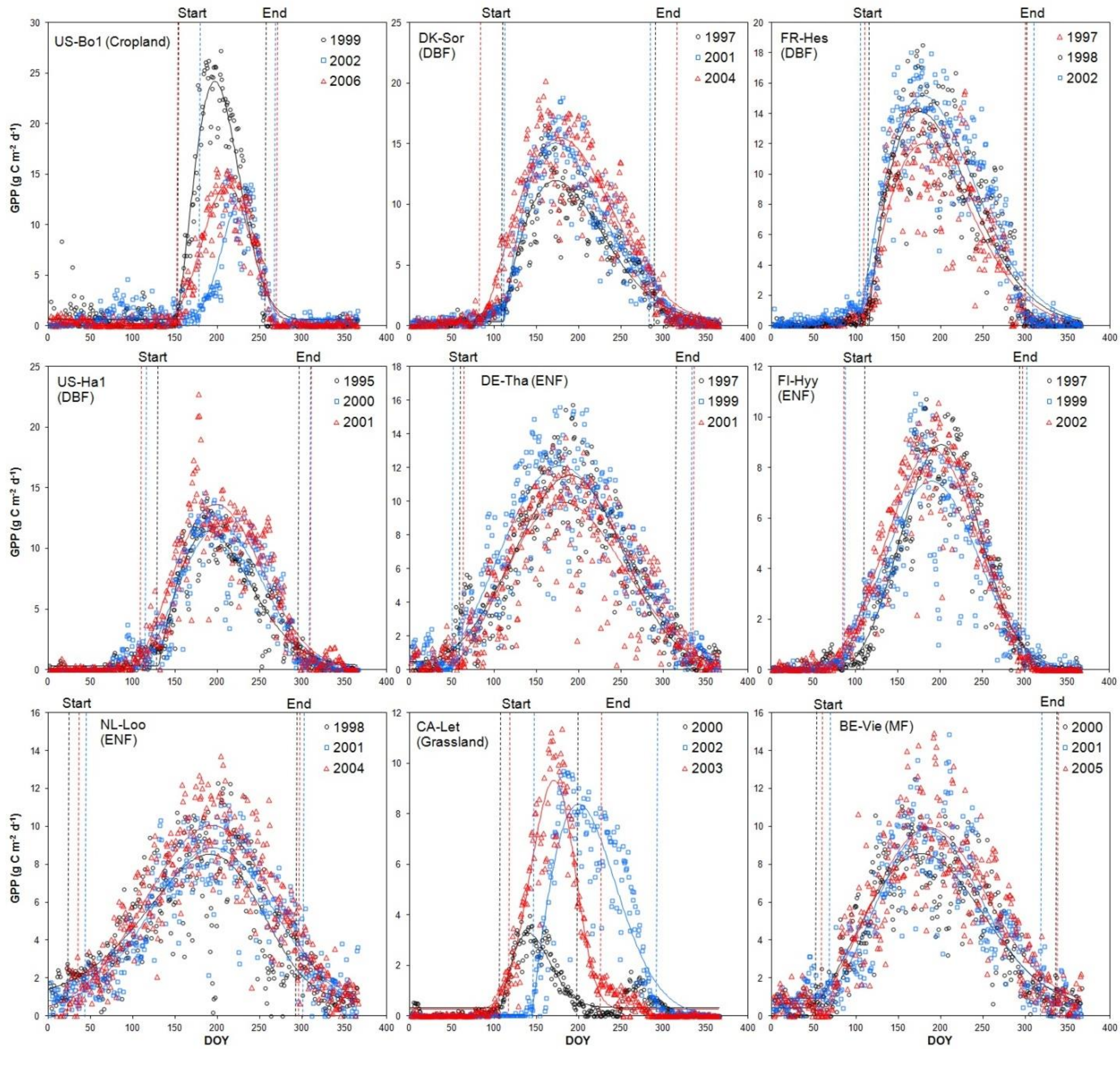

Supplementary Fig. S1.5.1. Performance of the Weibull function in fitting the GPP dynamics with lowest (black circles and lines), median (blue circles and lines) and highest (red circles and lines) annual GPP in those long-term flux sites. The dashed vertical lines represent the start and end days of CUP.

S1.6 Parameter sensitivity analysis of the Weibull function

In order to test if the convergence of α is a mathematical certainty of the Weibull function, we performed a sensitivity analysis to evaluate impact of each parameter ($x0$, $y0$, a, b, and c) on the estimates of CUP, GPP_{max}, CUP $\times GPP_{max}$, and α. The mathematical derivation of the sensitivity analysis can be found as follows:

We first assume $v = \left| \frac{t-x0}{b} + \left(\frac{c-1}{c}\right)^{\frac{1}{c}} \right|$, so then the above equation can be rewritten as:

$$P(t) = \begin{cases} y0 + a\left(\frac{c-1}{c}\right)^{\frac{1-c}{c}} v^{c-1} e^{\left(-v^{c} + \frac{c-1}{c}\right)} & if \;\; t \le x0 - b\frac{c-1}{c} \\ y0 & if \;\; t > x0 - b\frac{c-1}{c} \end{cases} \quad (23)$$

$P(t)$ is a differentiable function whose derivative is:

$$P(t)' = \begin{cases} a\left(\frac{c-1}{c}\right)^{\frac{1-c}{c}} e^{\frac{c-1}{c}} \left(v(t^{c-1} e^{-v^{c}}\right)' v' & if \;\; x \le x0 - b\frac{c-1}{c} \\ 0 & if \;\; x > x0 - b\frac{c-1}{c} \end{cases}$$

$$\Rightarrow \; P(t)' = \begin{cases} a\left(\frac{c-1}{c}\right)^{\frac{1-c}{c}} e^{\frac{c-1}{c}} \left(v^{c-1} e^{-v^{c}}\right)' v' & if \;\; x \le x0 - b\frac{c-1}{c} \\ 0 & if \;\; x > x0 - b\frac{c-1}{c} \end{cases}$$

$$\Rightarrow \; P(t)' = \begin{cases} a\left(\frac{c-1}{c}\right)^{\frac{1-c}{c}} e^{\frac{c-1}{c}} \left[(c-1)v^{c-2} e^{-v^{c}} - c v^{2(c-1)} e^{-v^{c}}\right] v' & if \;\; x \le x0 - b\frac{c-1}{c} \\ 0 & if \;\; x > x0 - b\frac{c-1}{c} \end{cases} \quad (24)$$

where $$v' = \begin{cases} \frac{1}{b} & if \;\; \frac{x-x0}{b} + \left(\frac{c-1}{c}\right)^{\frac{1}{c}} \ge 0 \\ -\frac{1}{b} & if \;\; \frac{x-x0}{b} + \left(\frac{c-1}{c}\right)^{\frac{1}{c}} < 0 \end{cases} \quad (25)$$

Similar to the equations (12) – (13), the maximal (R_{max}) and minimal (R_{min}) change rate of daily GPP are obtained by:

$$R_{max} = \max\ \{P(t)'\} \tag{26}$$

$$R_{min} = \min\ \{P(t)'\} \tag{27}$$

The CUP_{start} and CUP_{end} can be calculated by the equations (14) and (15), respectively. The CUP can be calculated as CUP_{end} minus CUP_{start}, and GPP_{max} as $\max\{P(t)\}$.

In the analysis, we first calculated the bootstrapping medians of all parameters from their estimations from the eddy-flux sites. Then, we increased each parameter from -100% to 100%, with an interval of 1%, of its calculated medians with other parameters kept at the estimated values from observations. Finally, we calculated CUP, GPP_{max}, CUP $\times GPP_{max}$ and α with each combination of parameters and plotted their dependences on each parameter in Fig. S1.6.1. The sensitivity analysis showed that GPP_{max} is very sensitive to the parameter *a* (Fig. S1.6.1a) of the Weibull function, while CUP is mainly affected by the parameters *b* and *c* (Fig. S1.6.1b). The parameters *a*, *b* and *c* together control the variations of the product of GPP_{max} and CUP (Fig. S1.6.1c). The ratio between annual GPP and the product of GPP_{max} and CUP (α) can be affected by each of the parameters (*a*, *b*, *c*, *x*0, and *y*0; Fig. S1.6.1d). It suggests the convergence of α is not the mathematical certainty the of the Weibull function used in this study.

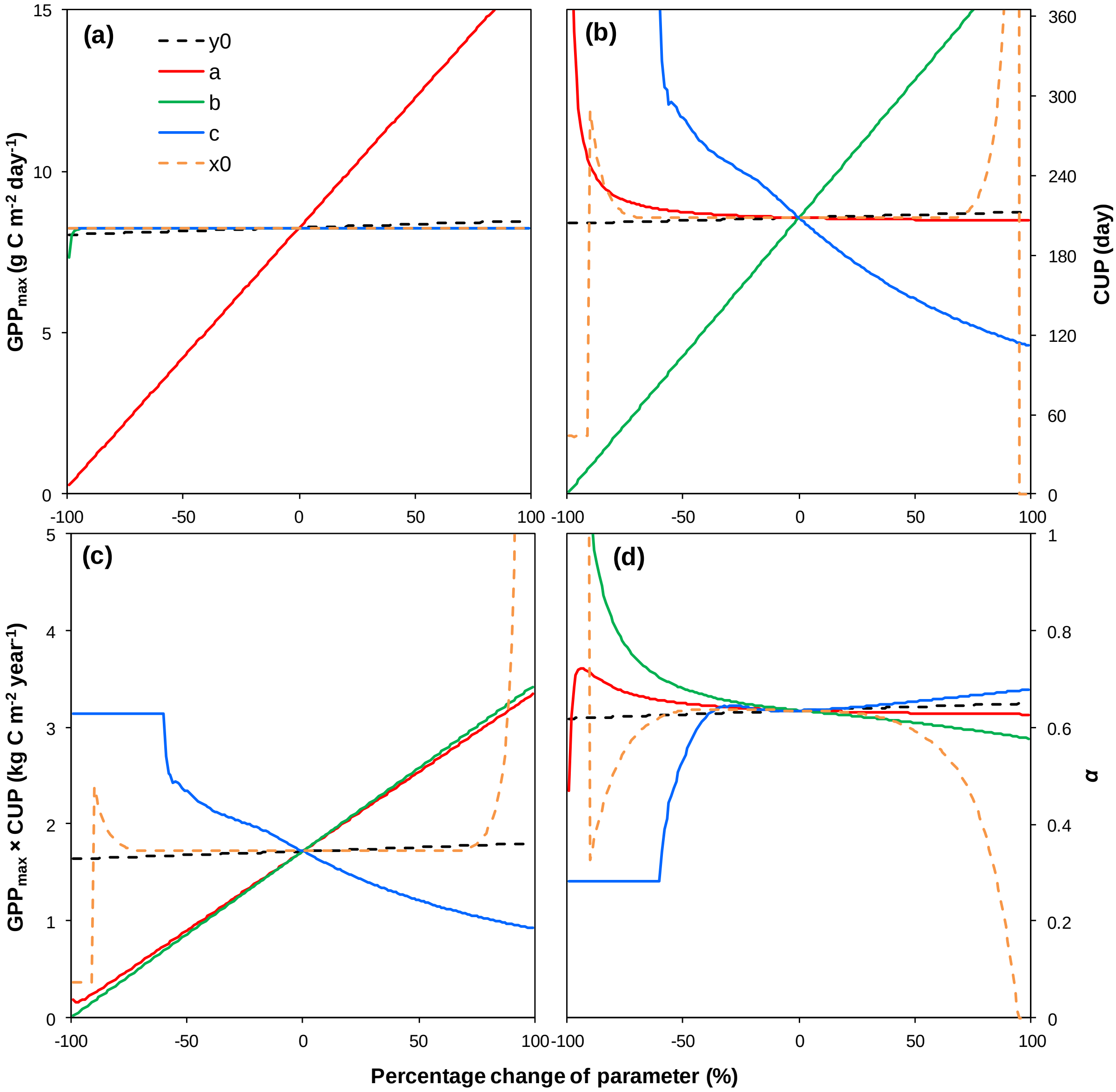

Supplementary Fig. S1.6.1. Sensitivity analyses of parameters. The results are obtained through the following steps: (1) calculate the bootstrapping median of the parameters from the global analyses on flux data; (2) change those parameters from -100% to +100% and calculate the values of GPP_{max}, CUP, GPP_{max} ×CUP, and α (annual GPP/(GPP_{max} ×CUP)) with equations (23) – (25).

S1.7 Random re-sampling test of the Weibull function

We further did a random re-sampling test for the performance of the Weibull funtion itself in affecting the ratio between annual GPP and the product of CUP and GPP_{max} (α). The test consisted of three steps: First, we set up the ranges of each parameter (*a*, *b*, *c*, *x0*, and *y0*) in equation 7, with $0 < a \leq 30$, $0 < b \leq 500$, $1 < c \leq 5$, $0 < x0 \leq 300$, $0 < y0 \leq 2$. For each parameter, the given range covered > 90% of the estimated values from all FLUXNET sites. Second, we equally separated the range of each parameter into 10000 samples from the lowest to largest value. For example, there were 1000 samples of parameter *a* including 0.003, 0.006, ... , 30. In the third step, we randomly chose each parameter from its 10000 samples to obtain the CUP, GPP_{max}, and annual GPP and thus the α. The random resampling of parameters was repeated by 2000 times, and the output was used for the further analyses.

As shown by Fig. S1.7.1, annual GPP is positively related to the product of CUP and GPP_{max}. However, the ratio (α) between them diverges. By plotting the frequency distribution of α that ranges from 0 to 1, we found it follows the normal distribution ($R^2 = 0.85$, $P < 0.001$; Fig. S1.7.2). Since the ranges of parameters are chosen based on the estimates in the natural ecosystems, the highest frequency of α in random resampling test is close to that found in the original analysis (as shown in Fig. 1 of the main text). However the divergence of α suggests that the global convergence of α should be caused by ecological processes in the natural ecosystems, but not the Weibull function itself.

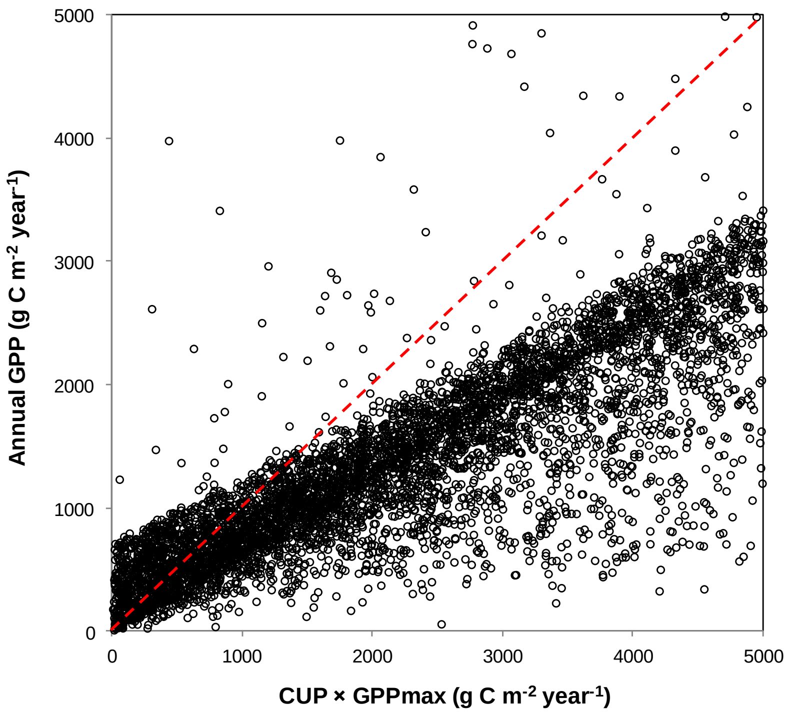

Supplementary Fig. S1.7.1. Results of a random re-sampling test. The parameter ranges were defined according to their distributions in the FLUXNET sites. The red dashed line is the 1:1 line.

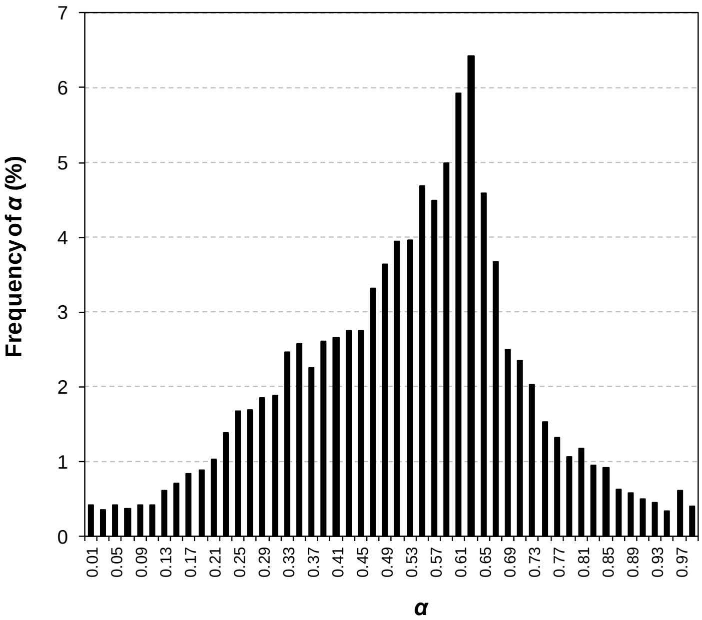

Supplementary Fig. S1.7.2. Frequency of α in the output of the random re-sampling test.

S1.8 Freeze/Thaw Data

Global daily records of landscape freeze/thaw data from 1st January 2000 to 31st December 2010 were analyzed for an additional indicator of CUP. The data were obtained from the NSIDC (http://nsidc.org/data/nsidc-0477). More detailed information about the data were provided at: http://nsidc.org/data/docs/measures/nsidc-0477/index.html. We used the combined freeze/thaw data (specifically, AM and PM thawed ground-state) to estimate dates of spring thaw and autumn freeze with the approach introduced by some earlier studies (24-26). The spring thaw data was defined as the date corresponding to the 8th day of the first 15 day period in a year when 80% days (i.e., 12 days) is classified as non-frozen days. The similar 80% rule was applied for determine the date of autumn freeze (i.e., end of CUP) for each grid. The global distribution of obtained CUP from the Freeze/Thaw (F/T) data was shown in Fig. S10.

S1.9 Distribution of FLUXNET Sites

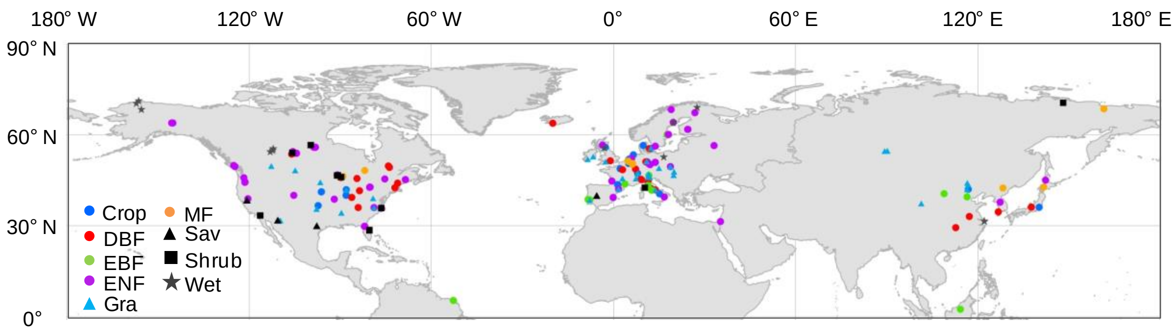

Supplementary Fig. S1.9.1. Distribution of FLUXNET sites that used in this study. Crop, cropland; DBF, deciduous broadleaf forest; EBF, evergreen broadleaf forest; ENF, evergreen needleleaf forest; MF, mixed forest; Gra, grassland, Sav, savanna; Shrub, shrubland; Wet, wetland.

As shown in Fig. S1.9.1, the eddy covariance sites are not homogeneously distributed over the global. More sites are distributed in North America, West Europe, and East Asia. Although the FLUXNET sites cannot fully represent the global heterogeneity in environmental conditions, they occupy almost all vegetation types and climate zones in terrestrial ecosystem (Please see more details in the Supporting Online Material of Beer et al.(5)). Our goal in this study is to test the control of phenological and physiological aspects on terrestrial annual GPP, so the broadly distributed FLUXNET sites are plenty to represent most vegetation and climate types in terrestrial ecosystems.

S2. Supplementary Tables and Figures

Table S1. Information of FLUXNET sites used in this study.

Site Name	PFT	Lat	Lon	Year	Ref.
AT-Neu	Grassland	47.1	11.3	2002-2006	(27)
BE-Bra	MF	51.3	4.5	1997-1998,2000-2002,2004-2006	(28)
BE-Lon	Cropland	50.6	4.7	2004-2006	(29)
BE-Vie	MF	50.3	6.0	1997-2006	(30)
BR-Sa1	EBF	-2.85	-54.97	2001-2003	(31)
BR-Sa3	EBF	-3.02	-54.97	2001-2003	(32)
BR-Sp1	Savanna	-21.6	-47.7	2001	(33)
CA-Ca1	ENF	49.9	-125.3	1998-2005	(34)
CA-Ca2	ENF	49.9	-125.3	2001-2005	(34)
CA-Ca3	ENF	49.5	-124.9	2002-2005	(34)
CA-Gro	MF	48.2	-82.2	2004	(35)
CA-Let	Grassland	49.7	-112.9	1999-2005	(36)
CA-Man	ENF	55.9	-98.5	1995,1998-2000	(37)
CA-Mer	ENF	45.4	-75.5	1999-2005	(38)
CA-NS1	ENF	55.9	-98.5	2003-2005	(39)
CA-NS2	ENF	55.9	-98.5	2002-2005	(39)
CA-NS3	ENF	55.9	-98.4	2002-2005	(39)
CA-NS4	ENF	55.9	-98.4	2003-2004	(39)
CA-NS5	ENF	55.9	-98.5	2002-2005	(39)
CA-NS6	ENF	55.9	-99.0	2002-2005	(39)
CA-NS7	Shrubland	56.6	-99.9	2003-2005	(39)

CA-Oas	DBF	53.6	-106.2	1997-2005	(40)
CA-Ojp	DBF	53.9	-104.7	2000-2003,2005	(41)
CA-Qcu	DBF	49.3	-74.0	2002-2006	(42)
CA-Qfo	DBF	49.7	-74.3	2004-2006	(43)
CA-SF1	ENF	54.5	-105.8	2004	(44)
CA-SF2	ENF	54.3	-105.9	2003-2004	(44)
CA-SF3	Shrubland	54.1	-106.0	2003-2005	(44)
CA-SJ1	ENF	53.9	-104.7	2001-2005	(45)
CA-SJ2	ENF	53.9	-104.6	2003-2005	(45)
CA-SJ3	ENF	53.9	-104.6	2004-2005	(45)
CA-TP1	ENF	42.7	-80.6	2004-2005	(46)
CA-TP2	ENF	42.8	-80.5	2004-2005	(46)
CA-TP3	ENF	42.7	-80.3	2005	(46)
CA-TP4	ENF	42.7	-80.4	2004-2005	(47)
CA-WP1	Wetland	55.0	-112.5	2004-2005	(48)
CA-WP2	Wetland	55.5	-112.3	2004	(49)
CA-WP3	Wetland	54.5	-113.3	2004	(49)
CH-Oe1	Grassland	47.3	7.7	2002-2006	(50)
CH-Oe2	Cropland	47.3	7.7	2005	(51)
CN-Anh	DBF	33.0	117.0	2005-2006	(52)
CN-Bed	EBF	39.5	116.3	2005	(52)
CN-Cha	MF	42.4	128.1	2003	(53)
CN-Do1	Wetland	31.5	122.0	2005	(54)
CN-Do2	Wetland	31.6	121.9	2005	(54)
CN-Do3	Wetland	31.5	122.0	2005	(54)
CN-Du1.	Cropland	42.0	116.7	2005-2006	(55)
CN-Du2	Grassland	42.0	116.3	2006	(55)
CN-HaM	Grassland	37.4	101.2	2002-2003	(56)
CN-Hny	DBF	29.3	112.5	2005-2006	–
CN-Ku1	EBF	40.5	108.7	2006	(57)
CN-Xfs	Grassland	44.1	116.3	2004-205	–
CZ-BK1	ENF	49.5	18.5	2001,2004-2006	–
CZ-BK2	Grassland	49.5	18.5	2005-2006	–
CZ-wet	Grassland	49.0	14.8	2006	(58)
DE-Bay	ENF	50.1	11.9	1997-1999	(59)
DE-Geb	Cropland	51.1	10.9	2004-2006	(60)
DE-Gri	Cropland	50.9	13.5	2005-2006	(16)
DE-Hai	DBF	51.1	10.5	2000-2006	(61)
DE-Har	DBF	51.1	10.5	2005-2006	(62)
DE-Kli	Cropland	50.9	13.5	2005-2006	–
DE-Meh	Grassland	51.3	10.7	2004-2006	(63)
DE-Tha	ENF	51.0	13.6	1997-2006	(64)
DE-Wet	ENF	50.5	11.5	2002-2006	(65)
DK-Fou	Cropland	56.5	9.6	2005	–
DK-Lva	Grassland	55.7	12.1	2005-2006	(16)

DK-Ris	Cropland	55.5	12.1	2004-2005	(66)
DK-Sor	DBF	55.5	11.6	1996-2006	(66)
ES-ES1	ENF	39.3	-0.3	1999-2002,2004-2006	(3)
ES-ES2	Cropland	39.3	-0.3	2004-2006	–
ES-LMa	Savanna	39.9	-5.8	2004-2006	(67)
ES-VDA	Grassland	42.2	1.4	2004-2005	(61)
FI-Hyy	ENF	61.8	24.3	1997-2006	(68)
FI-Kaa	Wetland	69.1	27.3	2000-2006	(69)
FI-Sii	ENF	61.8	24.2	2004-2005	(70)
FI-Sod	ENF	67.4	26.6	2000-2006	(71)
FR-Aur	Cropland	43.5	1.1	2005	–
FR-Fon	DBF	48.5	2.8	2005-2006	–
FR-Gri	Cropland	48.8	2.0	2005-2006	(72)
FR-Hes	DBF	48.7	7.1	1997-2006	(73)
FR-Lam	Cropland	43.5	1.2	2005	–
FR-LBr	ENF	44.7	-0.8	1997-1998,2000,2004-2006	(74)
FR-Lq1	Grassland	45.6	2.7	2004-2006	(16)
FR-Lq2	Grassland	45.6	2.7	2004-2006	(16)
FR-Pue	EBF	43.7	3.6	2001-2006	(75)
GF-Guy	EBF	5.3	-52.9	2005-2006	(76)
HU-Bug	Grassland	46.7	19.6	2003-2006	(77)
HU-Mat	Grassland	47.8	19.7	2004-2006	(78)
ID-Pag	EBF	2.3	114.0	2002-2003	(79)
IE-Ca1	Grassland	52.9	-6.9	2004-2006	–
IE-Dri	Grassland	52.0	-8.8	2003-2004	(80)
IL-Yat	ENF	31.3	35.1	2001-2006	(21)
IS-Gun	DBF	63.8	-20.2	1997-1998	(81)
IT-Amp	Grassland	41.9	13.6	2003-2006	(16)
IT-BCi	Cropland	40.5	15.0	2004-2006	(82)
IT-Bon	ENF	39.5	16.5	2006	–
IT-Col	DBF	41.8	13.6	1997-2005	(83)
IT-Cpz	EBF	41.7	12.4	1997,2001,2003-2006	(84)
IT-Lav	ENF	39.5	16.5	2001-2002,2004,2006	(85)
IT-Lec	EBF	43.3	11.3	2006	–
IT-LMa	Grassland	45.6	7.2	2003-2005	–
IT-Mal	Grassland	46.1	11.7	2003	–
IT-MBo	Grassland	46.0	11.0	2003-2006	(86)
IT-Non	DBF	44.7	11.1	2001-2003,2006	–
IT-Pia	Shrubland	42.6	10.1	2002-2005	(87)
IT-PT1	DBF	45.2	9.1	2002-2004	(88)
IT-Ren	EBF	46.6	11.4	1999,2001-2006	(89)
IT-Ro1	DBF	42.4	11.9	2001-2006	(90)
IT-Ro2	DBF	42.4	11.9	2002-2006	(91)
IT-SRo	ENF	39.5	16.5	1999-2006	(92)

IT-Vig	DBF	45.3	8.9	2005	–
JP-Mas	Cropland	36.1	140.0	2002-2003	(93)
JP-Tak	DBF	36.1	137.4	1999-2004	(94)
JP-Tef	ENF	45.1	142.1	2002,2004-2005	(95)
JP-Tom	MF	42.7	141.5	2001-2003	(96)
KR-Hnm	DBF	34.6	126.6	2004-2006	(97)
KR-Kw1	ENF	37.7	127.2	2005-2006	(98)
NL-Ca1	Grassland	52.0	4.9	2003-2006	(99)
NL-Hor	Grassland	52.0	5.1	2005-2006	(99)
NL-Lan	Cropland	52.0	4.9	2005	(99)
NL-Loo	ENF	52.2	5.7	1997-2006	(100)
NL-Lut	Cropland	53.4	6.4	2006	(101)
NL-Mol	Cropland	51.7	4.6	2005	(101)
PL-wet	Wetland	52.8	16.3	2004-2005	(102)
PT-Esp	EBF	38.6	-8.6	2002-2004,2006	(103)
PT-Mi1	EBF	38.5	-8.0	2003-2005	(104)
PT-Mi2	Grassland	38.5	-8.0	2006	(104)
RU-Che	MF	68.6	161.3	2003-2004	(105)
RU-Cok	Shrubland	70.6	147.9	2003	(106)
RU-Fyo	ENF	56.5	32.9	1998-2006	(107)
RU-Ha1	Grassland	54.7	90.0	2003-2004	(108)
RU-Ha3	Grassland	54.7	89.1	2004	(108)
RU-Zot	ENF	56.5	32.9	2002-2004	–
SE-Abi	ENF	68.4	18.8	2005	–
SE-Deg	Wetland	64.2	19.6	2001-2005	(109)
SE-Faj	ENF	56.3	13.6	2006	(110)
SE-Fla	ENF	64.1	19.5	1997-1998	(111)
SE-Fla	ENF	64.1	19.5	2001-2002	(111)
SE-Nor	EBF	60.1	17.5	1996-1999,2003	(112)
SE-Sk1	ENF	60.1	17.9	2005	–
SE-Sk2	ENF	60.1	17.8	2004-2005	–
UK-AMo	Wetland	55.8	-3.2	2005	(113)
UK-EBu	Grassland	55.9	-3.2	2004-2006	(114)
UK-ESa	Cropland	55.9	-2.9	2004-2005	–
UK-Gri	ENF	56.6	-3.8	1997-1998,2000-2001,2005-2006	(115)
UK-Ham	DBF	34.6	126.6	2004-2005	(116)
UK-PL3	DBF	51.5	-1.3	2005	–
UK-Tad	Grassland	51.2	-2.8	2001	(117)
US-ARb	Grassland	35.5	-98.0	2005-2006	–
US-ARc	Grassland	35.5	-98.0	2005-2006	–
US-ARM	Cropland	36.6	-97.5	2003-2006	(17)
US-Atq	Wetland	70.5	-157.4	2001,2003,2005-2006	(118)
US-Aud	Grassland	31.6	-110.5	2002,2005-2006	–
US-Bar	DBF	44.1	-71.3	2004-2005	(119)

US-Bkg	Grassland	44.3	-96.8	2005-2006	(120)
US-Blo	ENF	38.9	-120.6	2000-2006	(121)
US-Bn1	ENF	63.9	-145.4	2003	(122)
US-Bn2	ENF	63.9	-145.4	2003	(122)
US-Bn3	ENF	63.9	-145.7	2003	(122)
US-Bo1	Cropland	40.0	-88.3	1997-2006	(123)
US-Bo2	Cropland	40.0	-88.3	2004-2006	(123)
US-Brw	Wetland	71.3	-156.6	19,982,001	(124)
US-CaV	Grassland	39.1	-79.4	2004	–
US-Dk1	Grassland	36.0	-79.1	2002-2005	(125)
US-Dk2	DBF	36.0	-79.1	2003-2005	(125)
US-Dk3	ENF	36.0	-79.1	2001-2005	(125)
US-FPe	Grassland	48.3	-105.1	2000-2006	–
US-FR2	Savanna	29.9	-98.0	2004-2006	(126)
US-Goo	Grassland	34.3	-89.9	2002-2006	–
US-Ha1	DBF	42.5	-72.2	1992-2006	(127)
US-Ho1	ENF	45.2	-68.7	1996-2004	(128)
US-Ho2	ENF	45.2	-68.7	1999-2004	(128)
US-IB1	Cropland	41.9	-88.2	2006-2007	(129)
US-IB2	Grassland	41.8	-88.2	2006-2007	(129)
US-Ivo	Wetland	68.5	-155.8	2004-2006	–
US-KS2	Shrubland	28.6	-80.7	2001-2002,2004-2006	(130)
US-Los	Shrubland	46.1	-90.0	2001-2003,2005	–
US-LPH	DBF	42.5	-72.2	2003-2004	(131)
US-Me2	ENF	44.5	-121.6	2003-2005	(132)
US-Me3	ENF	44.3	-121.6	2004-2005	(132)
US-Me4	ENF	44.5	-121.6	1996-1997,2000	(132)
US-MMS	DBF	39.3	-86.4	1999-2005	(133)
US-NC1	Shrubland	35.8	-76.7	2005-2006	(134)
US-NC2	ENF	35.8	-76.7	2005-2006	(135)
US-Ne1	Cropland	41.2	-96.5	2001-2004	(136)
US-Ne2	Cropland	41.2	-96.5	2003-2004	(136)
US-Ne3	Cropland	41.2	-96.4	2001-2004	(136)
US-NR1	ENF	40.0	-105.5	1999-2000,2002-2003	(137)
US-Oho	DBF	41.6	-83.8	2004-2005	(138)
US-PFa	MF	45.9	-90.3	1997-2000,2003	(139)
US-SO2	Shrubland	33.4	-116.6	2004-2006	(140)
US-SO3	Shrubland	33.4	-116.6	20,012,005	(140)
US-SO4	Shrubland	33.4	-116.6	2005-2006	–
US-SP1	ENF	29.7	-82.2	2005	(141)
US-SP2	ENF	29.8	-82.2	1999-2004	(142)
US-SP3	ENF	29.8	-82.2	1999,2001-2004	(142)
US-SRM	Savanna	31.8	-110.9	2004-2006	(143)
US-Syv	MF	46.2	-89.3	2002-2006	(144)
US-Ton	Savanna	38.4	-121.0	2002-2006	(145)

US-UMB	DBF	45.6	-84.7	1999-2003	(146)
US-WBW	DBF	36.0	-84.3	1995-1999	(147)
US-WCr	DBF	45.8	-90.1	1999-2006	(148)
US-Wi0	ENF	46.6	-91.1	2002	(149)
US-Wi1	DBF	46.7	-91.2	2003	(150)
US-Wi2	ENF	46.7	-91.2	2003	(150)
US-Wi4	ENF	46.7	-91.2	2002-2005	(150)
US-Wi5	ENF	46.7	-91.1	2004	(150)
US-Wi6	Shrubland	46.6	-91.3	2002	(150)
US-Wi7	Shrubland	46.6	-91.1	2005	(150)
US-Wi8	DBF	46.7	-91.3	2002	(150)
US-Wkg	Grassland	31.7	-109.9	2005-2006	(151)
US-Wrc	ENF	45.8	-122.0	1999-2002,2004,2006	(152)
VU-Coc	EBF	-15.4	167.2	2002	(153)

Table S2. Results of partial correlation analyses for FLUXNET GPP. The dependent variable is annual GPP and independent variables are GPPmax and CUP.

	Variable entered	Parameter estimate	Patial r^2	Probability
All	GPP_{max}	0.98	0.72	<0.001
	CUP	0.96	0.26	<0.001
ENF	GPP_{max}	1.00	0.83	<0.001
	CUP	0.99	0.16	<0.001
DBF	GPP_{max}	1.00	0.87	<0.001
	CUP	0.99	0.11	<0.001
EBF	GPP_{max}	0.95	0.80	<0.001
	CUP	1.13	0.18	<0.001
MF	GPP_{max}	0.96	0.79	0.0014
	CUP	1.01	0.21	<0.001
GRA	GPP_{max}	1.00	0.70	0.005
	CUP	0.90	0.28	<0.001
SHRUB	GPP_{max}	0.90	0.52	0.0053
	CUP	1.06	0.43	<0.001
SAV	GPP_{max}	1.23	0.89	0.0014
	CUP	0.80	0.08	0.020
WET	GPP_{max}	1.02	0.91	<0.001
	CUP	0.82	0.08	0.002
CROP	CUP	0.88	0.58	0.0012
	GPPmax	0.86	0.37	<0.001

Figure S1. Relationship between GPP_{max} and CUP across all FLUXNET site-years in this study.

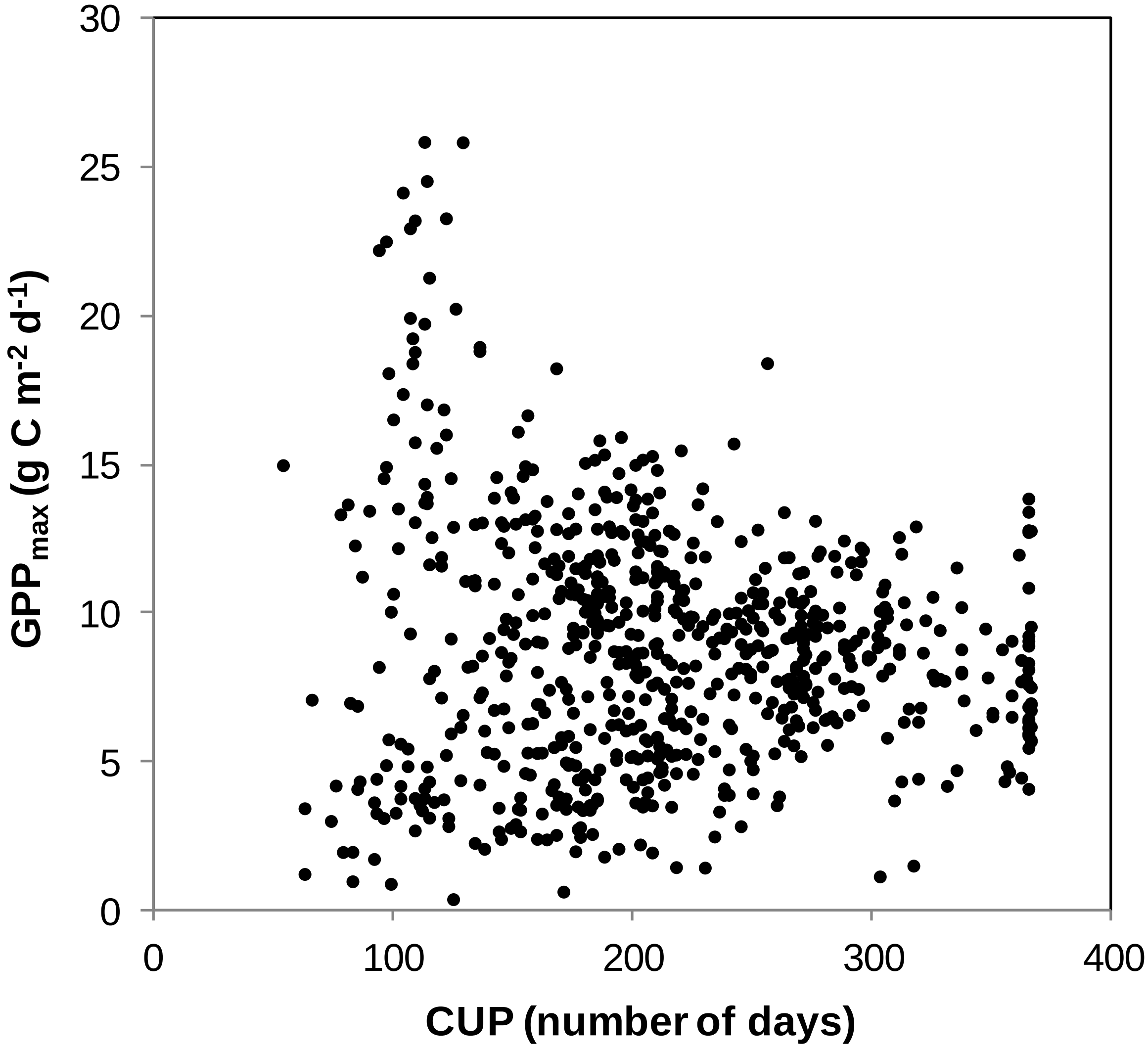

Figure S2. Dynamics of annual GPP, GPP_{max} and CUP from 2000 to 2010 in the Black Hills National Forest, South Dakota, USA. The results were obtained from the MODIS GPP observations in a 0.1 × 0.1° grid pixel (43.85°N, 103.95°W) which is located in the burned area in the Black Hills National Forest. More information about the fire disturbance and the following recovery of vegetation greenness can be found in Xiao *et al*.(154) . The linear regressions of annual GPP, GPP_{max} and CUP against year are all significant (all $P < 0.05$).

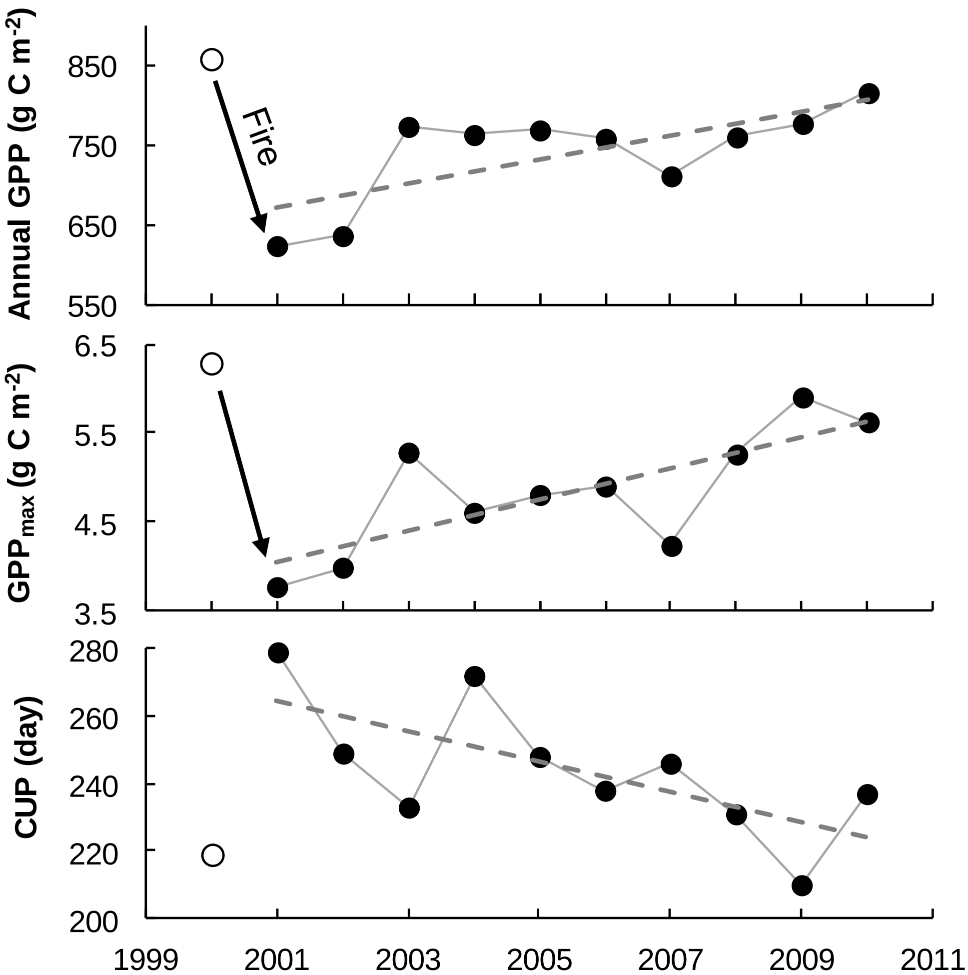

Figure S3. The relative frequency distribution of estimated α from all (a) non-tropical and (b) tropical and subtropical (including Mediterranean climate) FLUXNET site-years.

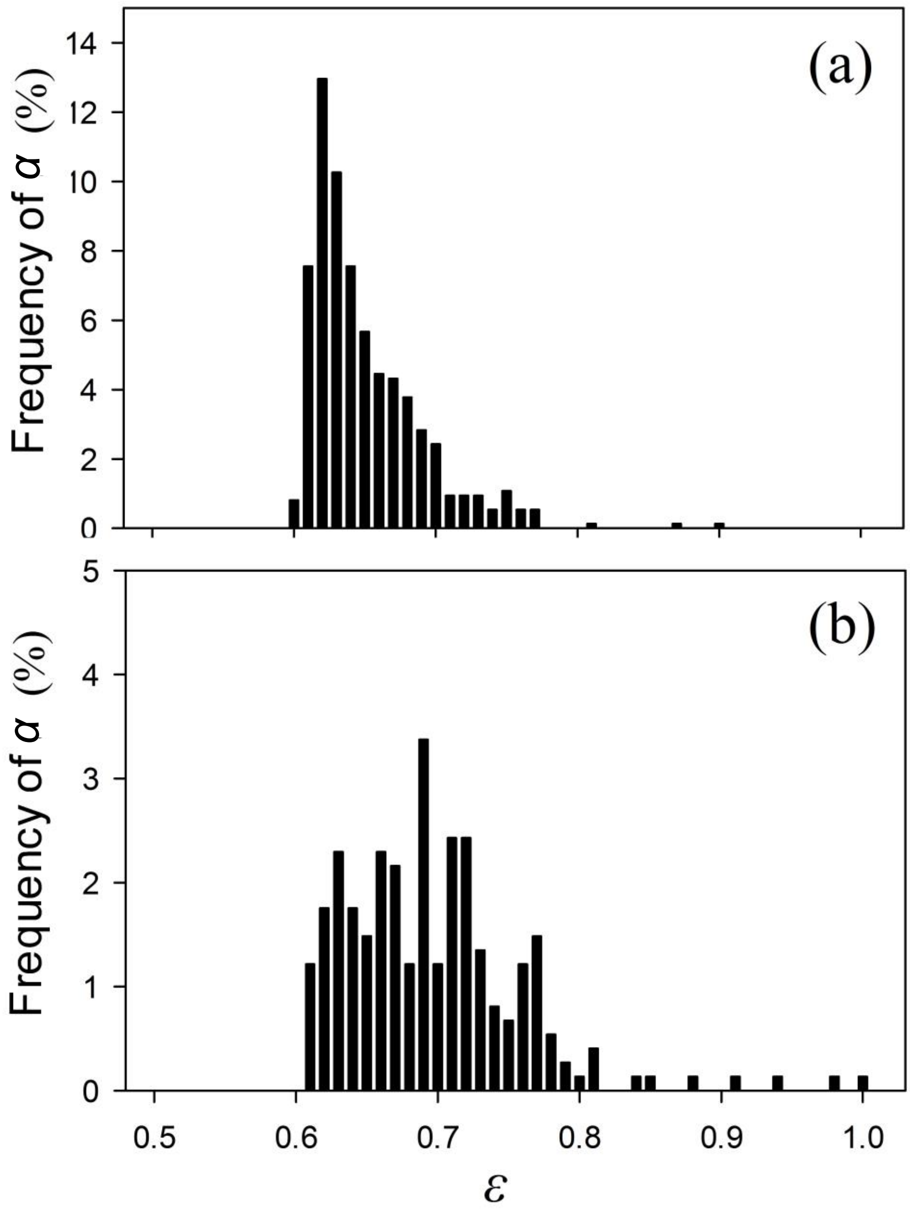

Figure S4. Spatial distributions of mean (a) annual GPP, (b) GPP_{max}, and (c) CUP in North America. Data in each 0.1 °×0.1 °grid was averaged over 11 years from 2000 to 2010.

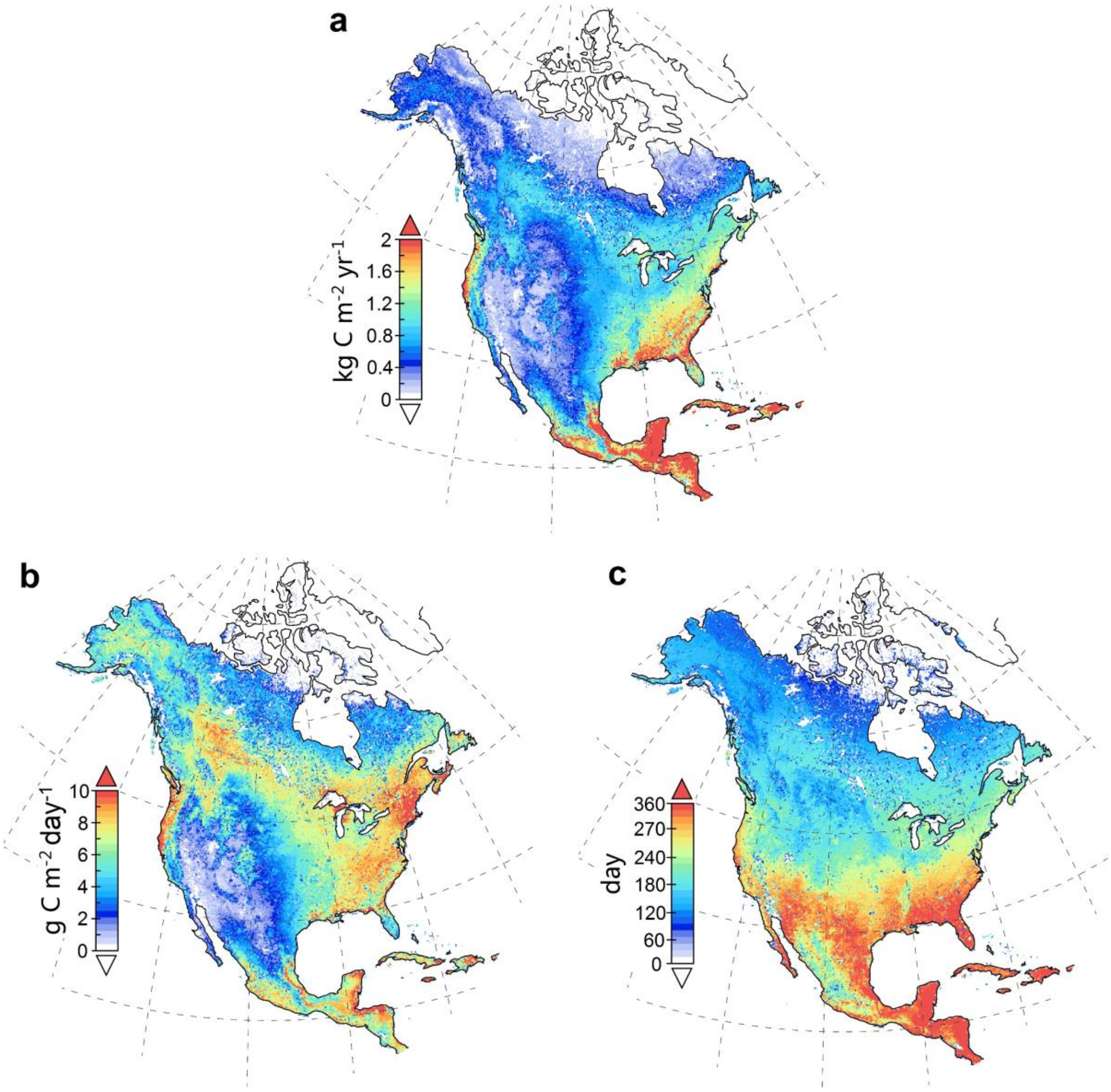

Figure S5. Examples of flux site-year with multiple peaks of daily GPP. Numbers and the associated arrows show the different GPP peaks. The detailed information for each flux site can be found in Table S1.

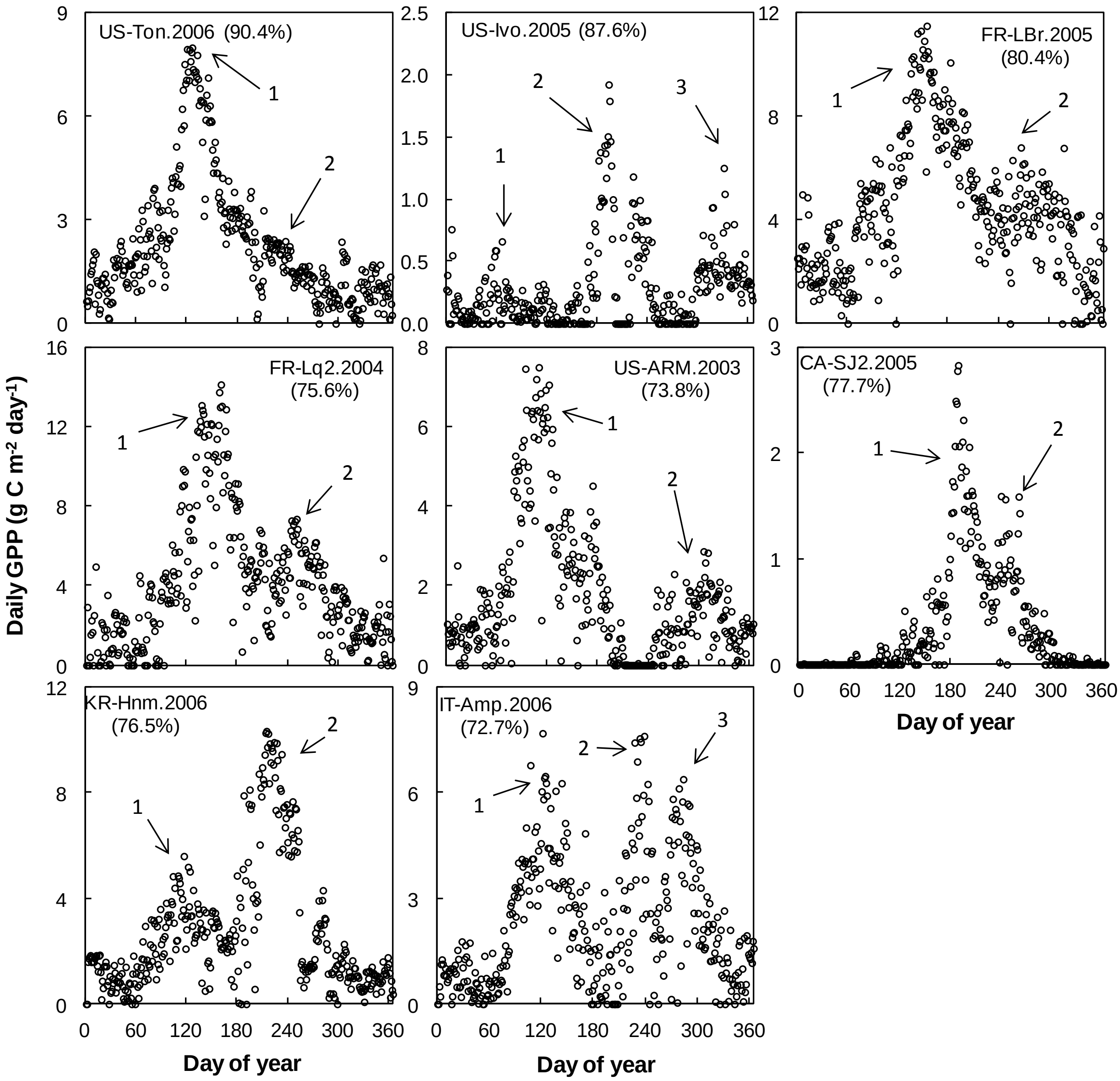

Figure S6. Dependence of annual FLUXNET GPP variability on (a) CUP and (b) GPP_{max} (the linear correlation was tested at the significance level of P = 0.05).

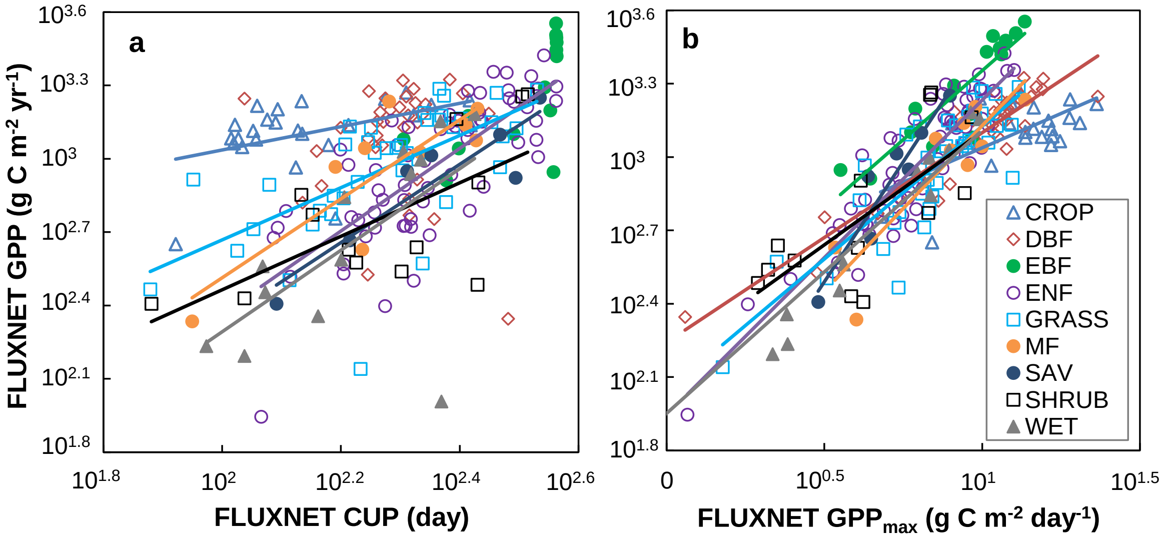

Figure S7. Relationship between MODIS- and FLUXNET-derived GPP_{max} in North America. The MODIS GPP_{max} (0.1 °by 0.1 °degree) from the latitude-longitude grid cell where the flux-tower site located was used for the analysis.

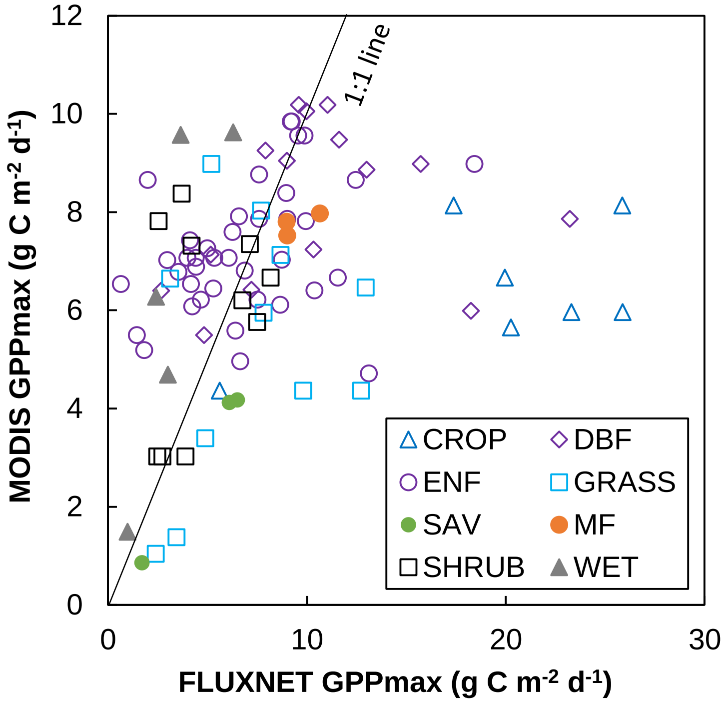

Figure S8. (a) Global distribution of averaged CUP over 2000-2010 derived from the daily records of landscape freeze/thaw (F/T) data with the spatial resolution of 25km by 25km. (b) Comparison between the MODIS- and F/T-derived CUP in North America. More details of the data and method are provided in S1.9. The F/T data were firstly re-gridded into 0.1 °by 0.1 °, and then both the MODIS- and F/T-derived were averaged along latitude with a 0.5 ° interval.

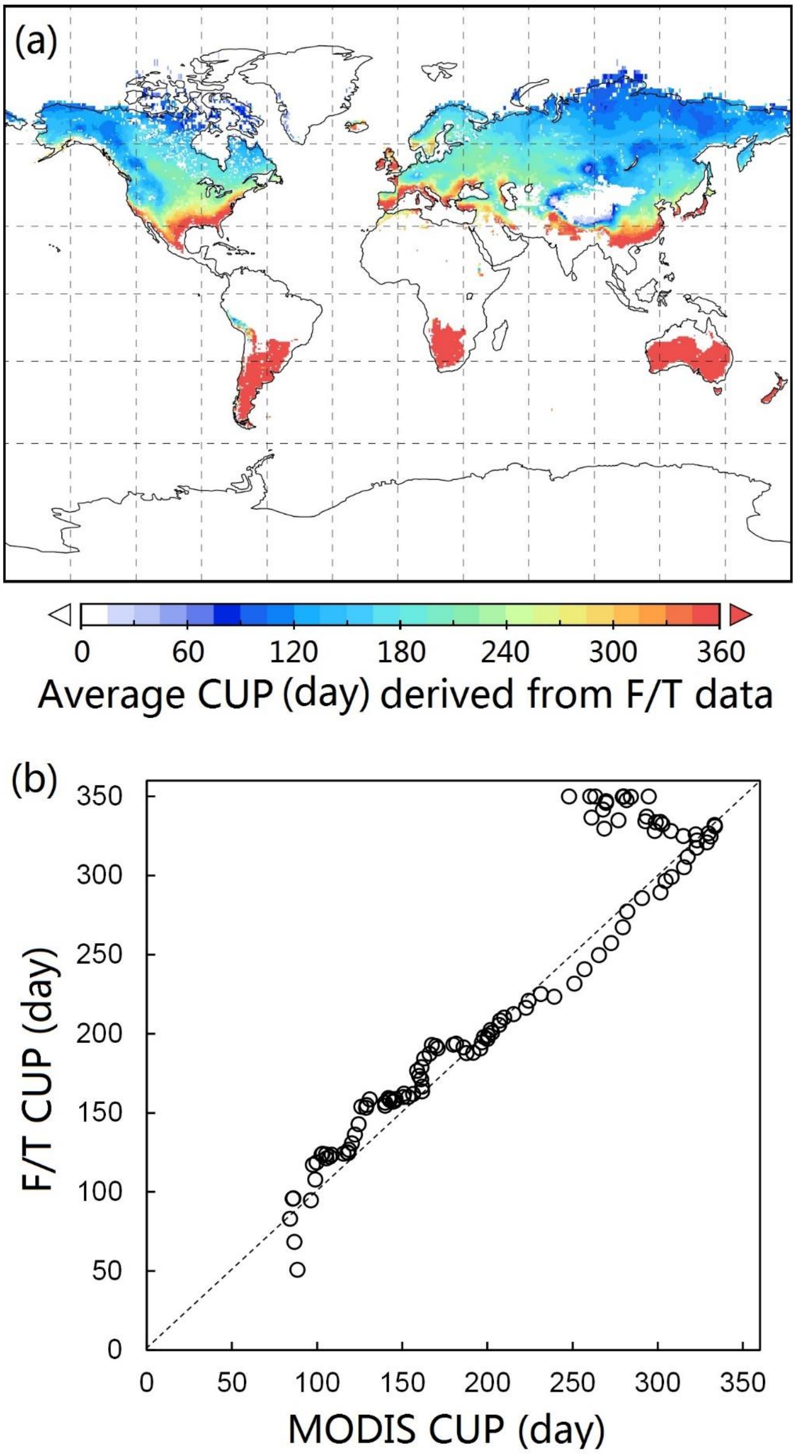

Figure S9. GPP dynamics in 2002 and 2003 at 10 FLUXNET sites in Europe. The year 2003 was extremely hot and dry, with July temperature up to 6 ℃ above and annual precipitation about 50% below the long-term averages(155). The selection of sites is based on the ref (149), which analyzed the impacts of the 2003 heatwave on European primary productivity. According to that study, GPP in 2002 (black triangle) was chosen as a reference and the impact of 2003 heatwave was calculated as the relative changes in 2003 (red circle) from those in 2002. The site information can be found in Table S1.

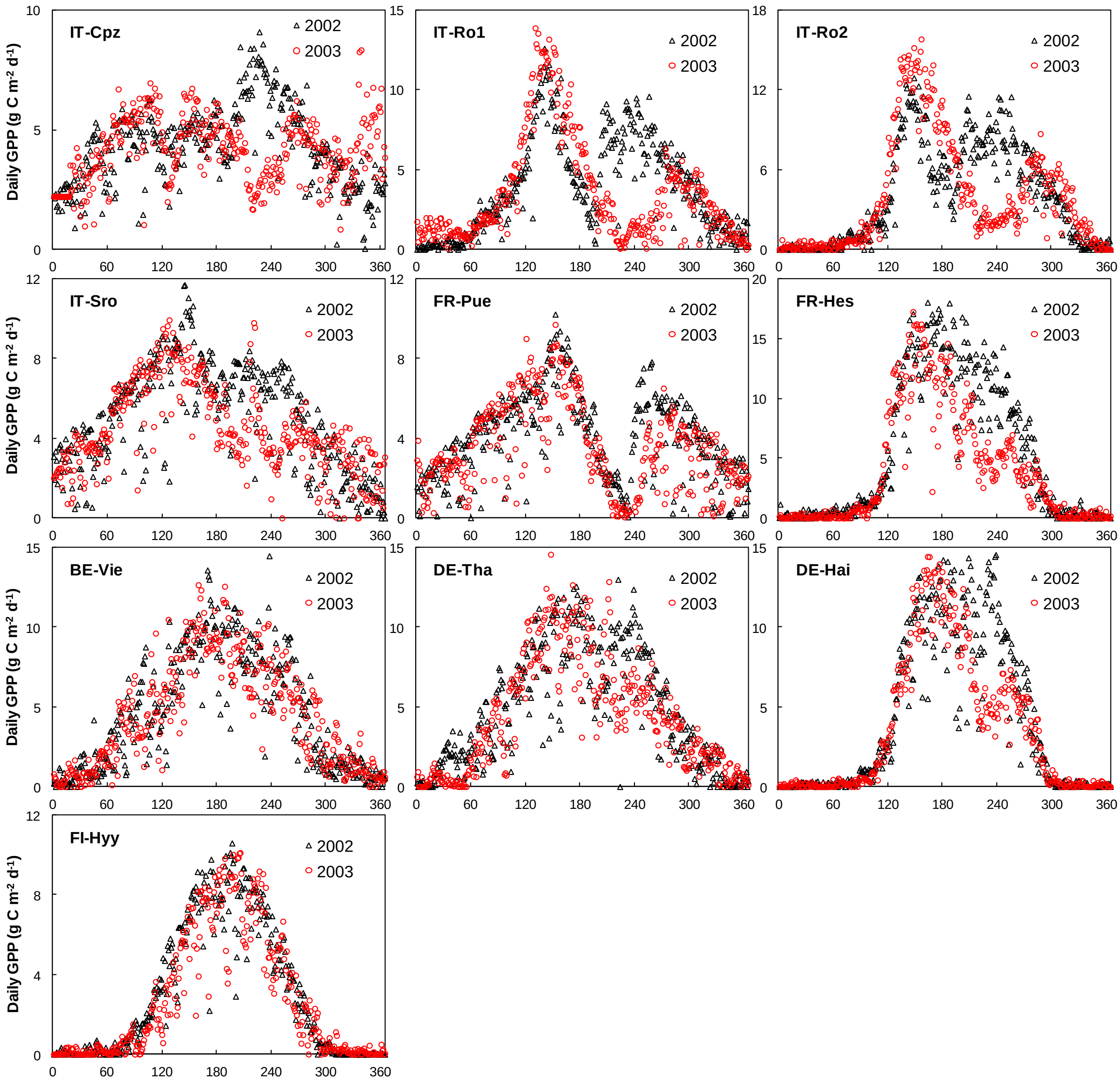

Figure S10. Relationship between annual GPP and the product of CUP and GPP_{max} in the Black Hills National Forest, South Dakota, USA. Each circle represents a year from 2000 to 2010. The results were obtained from the MODIS GPP observations in a 0.1×0.1^{o} grid pixel (43.85^{o}N, 103.95^{o}W) which located in the burned area in the Black Hills National Forest. More information about the fire disturbance and the following recovery of vegetation greenness can be found in Xiao *et al*.(154) .

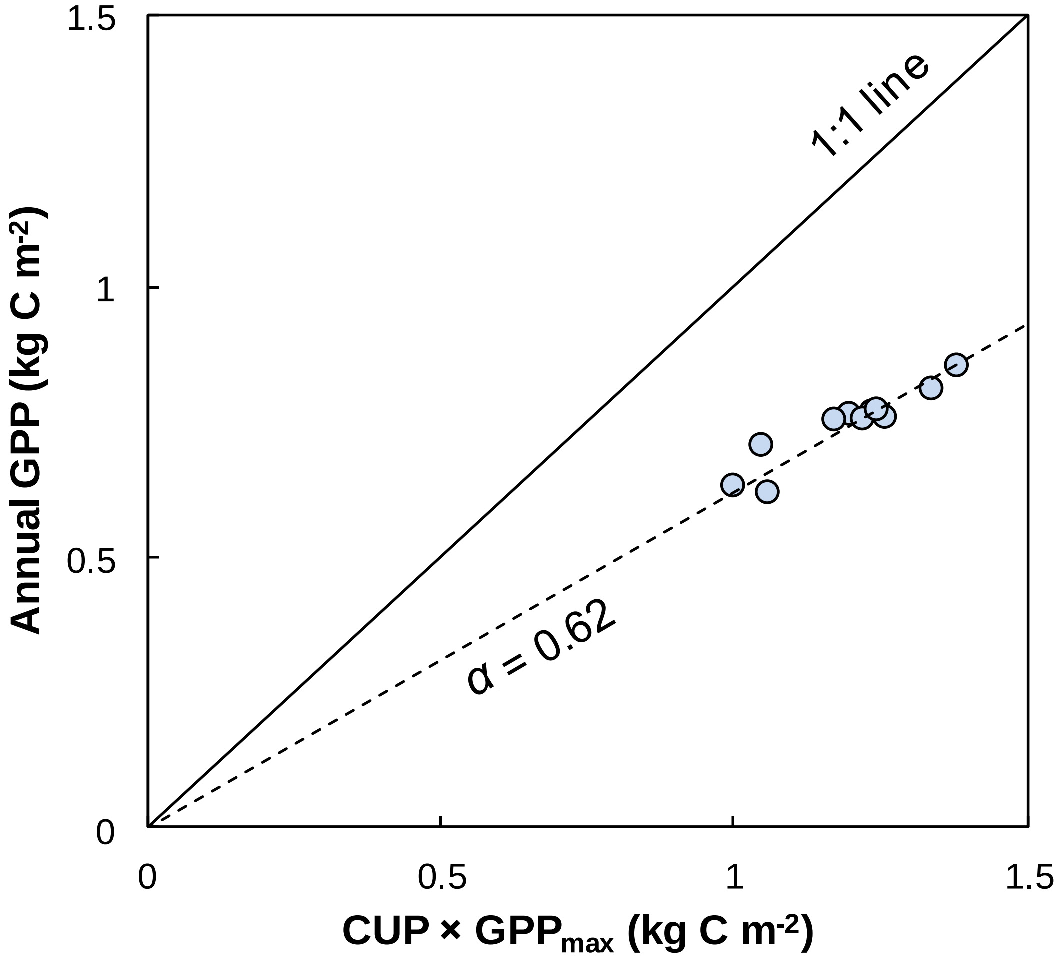

Supporting References

1. Baldocchi D, et al. (2001) FLUXNET: a new tool to study the temporal and spatial variability of ecosystem-scale carbon dioxide, water vapor, and energy flux densities. Bulletin of the American Meteorological Society 82(11):2415-2434.
2. Gu L, et al. (2003) Phenology of vegetation photosynthesis. Phenology: An integrative environmental science, (Springer), pp 467-485.
3. Reichstein M, et al. (2005) On the separation of net ecosystem exchange into assimilation and ecosystem respiration: review and improved algorithm. Global Change Biol 11(9):1424-1439.
4. Papale D, et al. (2006) Towards a standardized processing of Net Ecosystem Exchange measured with eddy covariance technique: algorithms and uncertainty estimation. Biogeosciences 3(4):571-583.
5. Beer C, et al. (2010) Terrestrial gross carbon dioxide uptake: global distribution and covariation with climate. Science 329(5993):834-838.
6. Moncrieff JB, Malhi Y, & Leuning R (1996) The propagation of errors in long-term measurements of land-atmosphere fluxes of carbon and water. Global Change Biol 2(3):231-240.
7. Moffat AM, et al. (2007) Comprehensive comparison of gap-filling techniques for eddy covariance net carbon fluxes. Agr Forest Meteorol 147(3-4):209-232.
8. Desai AR, et al. (2008) Cross-site evaluation of eddy covariance GPP and RE decomposition techniques. Agr Forest Meteorol 148(6-7):821-838.
9. Heinsch FA, et al. (2003) GPP and NPP (MOD17A2/A3) Products NASA MODIS Land Algorithm. MOD17 User's Guide:1-57.
10. Zhao MS, Heinsch FA, Nemani RR, & Running SW (2005) Improvements of the MODIS terrestrial gross and net primary production global data set. Remote Sens Environ 95(2):164-176.
11. Zhao MS & Running SW (2010) Drought-induced reduction in global terrestrial net primary production from 2000 Through 2009. Science 329(5994):940-943.
12. Running SW, et al. (2004) A continuous satellite-derived measure of global terrestrial primary production. Bioscience 54(6):547-560.
13. Sjostrom M, et al. (2011) Exploring the potential of MODIS EVI for modeling gross primary production across African ecosystems. Remote Sens Environ 115(4):1081-1089.
14. Gu L, et al. (2009) Characterizing the seasonal dynamics of plant community photosynthesis across a range of vegetation types. Phenology of Ecosystem Processes, (Springer), pp 35-58.
15. Jönsson P & Eklundh L (2004) TIMESAT—a program for analyzing time-series of satellite sensor data. Computers & Geosciences 30(8):833-845.
16. Gilmanov TG, et al. (2007) Partitioning European grassland net ecosystem CO_2 exchange into gross primary productivity and ecosystem respiration using light response function analysis. Agr Ecosyst Environ 121(1-2):93-120.

17. Fischer ML, Billesbach DP, Berry JA, Riley WJ, & Torn MS (2007) Spatiotemporal variations in growing season exchanges of CO_2, H_2O, and sensible heat in agricultural fields of the Southern Great Plains. Earth Interact 11, 10.1175/EI231.1

18. Liu XJ, Ju XT, Zhang FS, Pan JR, & Christie P (2003) Nitrogen dynamics and budgets in a winter wheat-maize cropping system in the North China Plain. Field Crop Res 83(2):111-124.

19. Eklundha L & Jönssonb P (2012) Timesat 3.1 Software Manual.

20. Giorgi F & Lionello P (2008) Climate change projections for the Mediterranean region. Global Planet Change 63(2-3):90-104.

21. Grunzweig JM, Lin T, Rotenberg E, Schwartz A, & Yakir D (2003) Carbon sequestration in arid-land forest. Global Change Biol 9(5):791-799.

22. Bates DM & Watts DG (1988) Nonlinear regression: iterative estimation and linear approximations (Wiley Online Library).

23. Fox J (2002) Nonlinear regression and nonlinear least squares. appendix to an R and S-PLUS companion to applied regression. (Sage Publications, Ca).

24. Xu L, et al. (2013) Temperature and vegetation seasonality diminishment over northern lands. Nature Climate Change 3(6):581-586.

25. Kim Y, Kimball JS, Zhang K, & McDonald KC (2012) Satellite detection of increasing Northern Hemisphere non-frozen seasons from 1979 to 2008: Implications for regional vegetation growth. Remote Sens Environ 121:472-487.

26. Zhang K, Kimball JS, Kim Y, & McDonald KC (2011) Changing freeze-thaw seasons in northern high latitudes and associated influences on evapotranspiration. Hydrol Process 25(26):4142-4151.

27. Wohlfahrt G, et al. (2008) Seasonal and inter-annual variability of the net ecosystem CO_2 exchange of a temperate mountain grassland: Effects of weather and management. J Geophys Res-Atmos 113, D08110, doi:10.1029/2007JD009286.

28. Carrara A, Janssens IA, Yuste JC, & Ceulemans R (2004) Seasonal changes in photosynthesis, respiration and NEE of a mixed temperate forest. Agr Forest Meteorol 126(1-2):15-31.

29. Moureaux C, Debacq A, Bodson B, Heinesch B, & Aubinet M (2006) Annual net ecosystem carbon exchange by a sugar beet crop. Agr Forest Meteorol 139(1-2):25-39.

30. Aubinet M, et al. (2001) Long term carbon dioxide exchange above a mixed forest in the Belgian Ardennes. Agr Forest Meteorol 108(4):293-315.

31. Tota J, et al. (2008) Amazon rain forest subcanopy flow and the carbon budget: Santarem LBA-ECO site. J Geophys Res-Biogeo 113, G00B02, doi:10.1029/2007JG000597.

32. Huete AR, et al. (2006) Amazon rainforests green-up with sunlight in dry season. Geophys Res Lett 33, L06405, doi:10.1029/2005GL025583.

33. da Rocha HR, et al. (2009) Patterns of water and heat flux across a biome gradient from tropical forest to savanna in Brazil. J Geophys Res-Biogeo 114, G00B12, doi:10.1029/2007JG000640.

34. Humphreys ER, et al. (2006) Carbon dioxide fluxes in coastal Douglas-fir stands at different stages of development after clearcut harvesting. Agr Forest Meteorol 140(1-4):6-22.

35. McCaughey JH, Pejam MR, Arain MA, & Cameron DA (2006) Carbon dioxide and energy fluxes from a boreal mixedwood forest ecosystem in Ontario, Canada. Agr Forest Meteorol 140(1-4):79-96.

36. Flanagan LB & Adkinson AC (2011) Interacting controls on productivity in a northern Great Plains grassland and implications for response to ENSO events. Global Change Biol 17(11):3293-3311.

37. Dunn AL, Barford CC, Wofsy SC, Goulden ML, & Daube BC (2007) A long-term record of carbon exchange in a boreal black spruce forest: means, responses to interannual variability, and decadal trends. Global Change Biol 13(3):577-590.

38. Lafleur PM, Roulet NT, Bubier JL, Frolking S, & Moore TR (2003) Interannual variability in the peatland-atmosphere carbon dioxide exchange at an ombrotrophic bog. Global Biogeochemical Cycles 1036, doi:10.1029/2002GB001983, 2.

39. Goulden ML, et al. (2004) Diel and seasonal patterns of tropical forest CO_2 exchange. Ecol Appl 14(4):S42-S54.

40. Black TA, et al. (2000) Increased carbon sequestration by a boreal deciduous forest in years with a warm spring. Geophys Res Lett 27(9):1271-1274.

41. Howard EA, Gower ST, Foley JA, & Kucharik CJ (2004) Effects of logging on carbon dynamics of a jack pine forest in Saskatchewan, Canada. Global Change Biol 10(8):1267-1284.

42. Giasson MA, Coursolle C, & Margolis HA (2006) Ecosystem-level CO_2 fluxes from a boreal cutover in eastern Canada before and after scarification. Agr Forest Meteorol 140(1-4):23-40.

43. Bergeron O, et al. (2007) Comparison of carbon dioxide fluxes over three boreal black spruce forests in Canada. Global Change Biol 13(1):89-107.

44. Mkhabela MS, et al. (2009) Comparison of carbon dynamics and water use efficiency following fire and harvesting in Canadian boreal forests. Agr Forest Meteorol 149(5):783-794.

45. Zha T, et al. (2009) Carbon sequestration in boreal jack pine stands following harvesting. Global Change Biol 15(6):1475-1487.

46. Peichl M & Arain MA (2007) Allometry and partitioning of above- and belowground tree biomass in an age-sequence of white pine forests. Forest Ecol Manag 253(1-3):68-80.

47. Yuan FM, et al. (2008) Modeling analysis of primary controls on net ecosystem productivity of seven boreal and temperate coniferous forests across a continental transect. Global Change Biol 14(8):1765-1784.

48. Flanagan LB & Syed KH (2011) Stimulation of both photosynthesis and respiration in response to warmer and drier conditions in a boreal peatland ecosystem. Global Change Biol 17(7):2271-2287.

49. Adkinson AC, Syed KH, & Flanagan LB (2011) Contrasting responses of growing season ecosystem CO_2 exchange to variation in temperature and water table depth in two

peatlands in northern Alberta, Canada. J Geophys Res-Biogeo 116, G01004, doi:10.1029/2010JG001512.

50. Ammann C, Flechard CR, Leifeld J, Neftel A, & Fuhrer J (2007) The carbon budget of newly established temperate grassland depends on management intensity. Agr Ecosyst Environ 121(1-2):5-20.
51. Dietiker D, Buchmann N, & Eugster W (2010) Testing the ability of the DNDC model to predict CO_2 and water vapour fluxes of a Swiss cropland site. Agr Ecosyst Environ 139(3):396-401.
52. Li X, et al. (2012) Estimation of evapotranspiration over the terrestrial ecosystems in China. Ecohydrology. 7: 139–149.
53. Guan DX, et al. (2006) CO_2 fluxes over an old, temperate mixed forest in northeastern China. Agr Forest Meteorol 137(3-4):138-149.
54. Yan Y, et al. (2008) Closing the carbon budget of estuarine wetlands with tower-based measurements and MODIS time series (vol 14, pg 1690, 2008). Global Change Biol 14(10):2469-2471.
55. Chen SP, et al. (2009) Energy balance and partition in Inner Mongolia steppe ecosystems with different land use types. Agr Forest Meteorol 149(11):1800-1809.
56. Kato T, et al. (2006) Temperature and biomass influences on interannual changes in CO_2 exchange in an alpine meadow on the Qinghai-Tibetan Plateau. Global Change Biol 12(7):1285-1298.
57. Sun G, et al. (2011) A general predictive model for estimating monthly ecosystem evapotranspiration. Ecohydrology 4(2):245-255.
58. Sulkava M, Luyssaert S, Zaehle S, & Papale D (2011) Assessing and improving the representativeness of monitoring networks: The European flux tower network example. J Geophys Res-Biogeo 116, G00J04, doi:10.1029/2010JG001562.
59. Staudt K & Foken T (2007) Documentation of reference data for the experimental areas of the bayreuth centre for ecology and environmental research (bayceer) at the waldstein site, Tech. Rep (University of Bayreuth).
60. Anthoni PM, et al. (2004) Forest and agricultural land-use-dependent CO_2 exchange in Thuringia, Germany. Global Change Biol 10(12):2005-2019.
61. Knohl A, Schulze ED, Kolle O, & Buchmann N (2003) Large carbon uptake by an unmanaged 250-year-old deciduous forest in Central Germany. Agr Forest Meteorol 118(3-4):151-167.
62. Schindler D, Turk M, & Mayer H (2006) CO_2 fluxes of a Scots pine forest growing in the warm and dry southern upper Rhine plain, SW Germany. Eur J Forest Res 125(3):201-212.
63. Don A, Rebmann C, Kolle O, Scherer-Lorenzen M, & Schulze ED (2009) Impact of afforestation-associated management changes on the carbon balance of grassland. Global Change Biol 15(8):1990-2002.
64. Grunwald T & Bernhofer C (2007) A decade of carbon, water and energy flux measurements of an old spruce forest at the Anchor Station Tharandt. Tellus B 59(3):387-396.

65. Rebmann C, et al. (2010) Treatment and assessment of the CO_2-exchange at a complex forest site in Thuringia, Germany. Agr Forest Meteorol 150(5):684-691.

66. Pilegaard K, et al. (2003) Field measurements of atmosphere-biosphere interactions in a Danish beech forest. Boreal Environ Res 8(4):315-333.

67. Gockede M, et al. (2008) Quality control of CarboEurope flux data - Part 1: Coupling footprint analyses with flux data quality assessment to evaluate sites in forest ecosystems. Biogeosciences 5(2):433-450.

68. Suni T, et al. (2003) Long-term measurements of surface fluxes above a Scots pine forest in Hyytiala, southern Finland, 1996-2001. Boreal Environ Res 8(4):287-301.

69. Laurila T, et al. (2001) Seasonal variations of net CO_2 exchange in European Arctic ecosystems. Theor Appl Climatol 70(1-4):183-201.

70. Aurela M, et al. (2007) CO_2 exchange of a sedge fen in southern Finland - The impact of a drought period. Tellus B 59(5):826-837.

71. Tanja S, et al. (2003) Air temperature triggers the recovery of evergreen boreal forest photosynthesis in spring. Global Change Biol 9(10):1410-1426.

72. Hibbard KA, Law BE, Reichstein M, & Sulzman J (2005) An analysis of soil respiration across northern hemisphere temperate ecosystems. Biogeochemistry 73(1):29-70.

73. Granier A, et al. (2000) The carbon balance of a young Beech forest. Funct Ecol 14(3):312-325.

74. Berbigier P, Bonnefond JM, & Mellmann P (2001) CO_2 and water vapour fluxes for 2 years above Euroflux forest site. Agr Forest Meteorol 108(3):183-197.

75. Rambal S, Joffre R, Ourcival JM, Cavender-Bares J, & Rocheteau A (2004) The growth respiration component in eddy CO_2 flux from a Quercus ilex mediterranean forest. Global Change Biol 10(9):1460-1469.

76. Bonal D, et al. (2008) Impact of severe dry season on net ecosystem exchange in the Neotropical rainforest of French Guiana. Global Change Biol 14(8):1917-1933.

77. Nagy Z, et al. (2007) The carbon budget of semi-arid grassland in a wet and a dry year in Hungary. Agr Ecosyst Environ 121(1-2):21-29.

78. Pinter K, et al. (2008) Interannual variability of grasslands' carbon balance depends on soil type. Community Ecol 9:43-48.

79. Hirano T, et al. (2007) Carbon dioxide balance of a tropical peat swamp forest in Kalimantan, Indonesia. Global Change Biol 13(2):412-425.

80. Peichl M, Leahy P, & Kiely G (2011) Six-year stable annual uptake of carbon dioxide in intensively managed humid temperate grassland. Ecosystems 14(1):112-126.

81. Morales P, et al. (2005) Comparing and evaluating process-based ecosystem model predictions of carbon and water fluxes in major European forest biomes. Global Change Biol 11(12):2211-2233.

82. Kutsch WL, et al. (2010) The net biome production of full crop rotations in Europe. Agr Ecosyst Environ 139(3):336-345.

83. Scartazza A, et al. (2004) Comparisons of d 13C of photosynthetic products and ecosystem respiratory CO_2 and their responses to seasonal climate variability. Oecologia 140(2):340-351.

84. Garbulsky MF, Penuelas J, Papale D, & Filella I (2008) Remote estimation of carbon dioxide uptake by a Mediterranean forest. Global Change Biol 14(12):2860-2867.

85. Marcolla B, Pitacco A, & Cescatti A (2003) Canopy architecture and turbulence structure in a coniferous forest. Bound-Lay Meteorol 108(1):39-59.

86. Marcolla B & Cescatti A (2005) Experimental analysis of flux footprint for varying stability conditions in an alpine meadow. Agr Forest Meteorol 135(1-4):291-301.

87. Vaccari FP, et al. (2012) Land use change and soil organic carbon dynamics in Mediterranean agro-ecosystems: The case study of Pianosa Island. Geoderma 175:29-36.

88. Migliavacca M, et al. (2009) Modeling gross primary production of agro-forestry ecosystems by assimilation of satellite-derived information in a process-based model. Sensors-Basel 9(2):922-942.

89. Montagnani L, et al. (2009) A new mass conservation approach to the study of CO_2 advection in an alpine forest. J Geophys Res-Atmos 114, D07306, doi:10.1029/2008JD010650.

90. Rey A, et al. (2002) Annual variation in soil respiration and its components in a coppice oak forest in Central Italy. Global Change Biol 8(9):851-866.

91. Tedeschi V, et al. (2006) Soil respiration in a Mediterranean oak forest at different developmental stages after coppicing. Global Change Biol 12(1):110-121.

92. Chiesi M, et al. (2005) Modelling carbon budget of Mediterranean forests using ground and remote sensing measurements. Agr Forest Meteorol 135(1-4):22-34.

93. Saito M, Miyata A, Nagai H, & Yamada T (2005) Seasonal variation of carbon dioxide exchange in rice paddy field in Japan. Agr Forest Meteorol 135(1-4):93-109.

94. Ito A, et al. (2006) Seasonal variation in leaf properties and ecosystem carbon budget in a cool-temperate deciduous broad-leaved forest: simulation analysis at Takayama site, Japan. Ecol Res 21(1):137-149.

95. Takagi K, et al. (2009) Change in CO_2 balance under a series of forestry activities in a cool-temperate mixed forest with dense undergrowth. Global Change Biol 15(5):1275-1288.

96. Hirano T, et al. (2003) CO_2 and water vapor exchange of a larch forest in northern Japan. Tellus B 55(2):244-257.

97. Choi M, Lee SO, & Kwon H (2010) Understanding of the Common Land Model performance for water and energy fluxes in a farmland during the growing season in Korea. Hydrol Process 24(8):1063-1071.

98. Kang M, Kwon H, Cheon JH, & Kim J (2012) On estimating wet canopy evaporation from deciduous and coniferous forests in the Asian monsoon climate. J Hydrometeorol 13(3):950-965.

99. Jacobs CMJ, et al. (2007) Variability of annual CO_2 exchange from Dutch grasslands. Biogeosciences 4(5):803-816.

100. Dolman AJ, Moors EJ, & Elbers JA (2002) The carbon uptake of a mid latitude pine forest growing on sandy soil. Agr Forest Meteorol 111(3):157-170.

101. Moors EJ, et al. (2010) Variability in carbon exchange of European croplands. Agr Ecosyst Environ 139(3):325-335.

102. Chojnicki B, Urbaniak M, Józefczyk D, Augustin J, & Olejnik J (2007) Measurements of gas and heat fluxes at Rzecin wetland. Wetlands: Monitoring, Modeling and Management, edited by Okruszko, T., Maltby, E., Szatylowicz, J., Miroslaw-Swiatek, D., and Kotowski, W:125-131.

103. Pital G, Rodrigues A, Mateus J, & Pereira J (2011) Reversing of seasonal patterns of carbon uptake in an eucalyptus stand in Portugal after drought and felling. Forest Syst 20(3):475-484.

104. Pereira J, et al. (2007) Net ecosystem carbon exchange in three contrasting Mediterranean ecosystems–the effect of drought. Biogeosciences 4:791-802.

105. Merbold L, et al. (2009) Artificial drainage and associated carbon fluxes (CO_2/CH_4) in a tundra ecosystem. Global Change Biol 15(11):2599-2614.

106. van der Molen MK, et al. (2007) The growing season greenhouse gas balance of a continental tundra site in the Indigirka lowlands, NE Siberia. Biogeosciences 4(6):985-1003.

107. Kurbatova J, Li C, Varlagin A, Xiao X, & Vygodskaya N (2008) Modeling carbon dynamics in two adjacent spruce forests with different soil conditions in Russia. Biogeosciences 5(4):969-980.

108. Marchesini LB, et al. (2007) Carbon balance assessment of a natural steppe of southern Siberia by multiple constraint approach. Biogeosciences 4(4):581-595.

109. Sagerfors J, et al. (2008) Annual CO_2 exchange between a nutrient-poor, minerotrophic, boreal mire and the atmosphere. J Geophys Res-Biogeo 113, G01001, doi:10.1029/2006JG000306.

110. Eklundh L, Jin HX, Schubert P, Guzinski R, & Heliasz M (2011) An optical sensor network for vegetation phenology monitoring and satellite data calibration. Sensors-Basel 11(8):7678-7709.

111. Lindroth A, Klemedtsson L, Grelle A, Weslien P, & Langvall O (2008) Measurement of net ecosystem exchange, productivity and respiration in three spruce forests in Sweden shows unexpectedly large soil carbon losses. Biogeochemistry 89(1):43-60.

112. Lagergren F, et al. (2008) Biophysical controls on CO_2 fluxes of three Northern forests based on long-term eddy covariance data. Tellus B 60(2):143-152.

113. Hargreaves K, Milne R, & Cannell M (2003) Carbon balance of afforested peatland in Scotland. Forestry 76(3):299-317.

114. Soussana JF, et al. (2007) Full accounting of the greenhouse gas (CO_2, N_2O, CH_4) budget of nine European grassland sites. Agr Ecosyst Environ 121(1-2):121-134.

115. Rebmann C, et al. (2005) Quality analysis applied on eddy covariance measurements at complex forest sites using footprint modelling. Theor Appl Climatol 80(2-4):121-141.

116. Wilkinson M, Eaton EL, Broadmeadow MSJ, & Morison JIL (2012) Inter-annual variation of carbon uptake by a plantation oak woodland in south-eastern England. Biogeosciences 9(12):5373-5389.

117. Acreman MC, Harding RJ, Lloyd CR, & McNeil DD (2003) Evaporation characteristics of wetlands: experience from a wet grassland and a reedbed using eddy correlation measurements. Hydrol Earth Syst Sc 7(1):11-21.

118. Kwon HJ, Oechel WC, Zulueta RC, & Hastings SJ (2006) Effects of climate variability on carbon sequestration among adjacent wet sedge tundra and moist tussock tundra ecosystems. J Geophys Res-Biogeo 111, G03014, doi:10.1029/2005JG000036.

119. Jenkins JP, et al. (2007) Refining light-use efficiency calculations for a deciduous forest canopy using simultaneous tower-based carbon flux and radiometric measurements. Agr Forest Meteorol 143(1-2):64-79.

120. Gilmanov TG, et al. (2005) Integration of CO_2 flux and remotely-sensed data for primary production and ecosystem respiration analyses in the Northern Great Plains: potential for quantitative spatial extrapolation. Global Ecol Biogeogr 14(3):271-292.

121. Goldstein AH, et al. (2000) Effects of climate variability on the carbon dioxide, water, and sensible heat fluxes above a ponderosa pine plantation in the Sierra Nevada (CA). Agr Forest Meteorol 101(2-3):113-129.

122. Liu HP, Randerson JT, Lindfors J, & Chapin FS (2005) Changes in the surface energy budget after fire in boreal ecosystems of interior Alaska: An annual perspective. J Geophys Res-Atmos 110, D13101, doi:10.1029/2004JD005158.

123. Meyers TP & Hollinger SE (2004) An assessment of storage terms in the surface energy balance of maize and soybean. Agr Forest Meteorol 125(1-2):105-115.

124. Oechel WC, et al. (2000) Acclimation of ecosystem CO_2 exchange in the Alaskan Arctic in response to decadal climate warming. Nature 406(6799):978-981.

125. Pataki DE & Oren R (2003) Species differences in stomatal control of water loss at the canopy scale in a mature bottomland deciduous forest. Adv Water Resour 26(12):1267-1278.

126. Heinsch FA, et al. (2004) Carbon dioxide exchange in a high marsh on the Texas Gulf Coast: effects of freshwater availability. Agr Forest Meteorol 125(1-2):159-172.

127. Urbanski S, et al. (2007) Factors controlling CO_2 exchange on timescales from hourly to decadal at Harvard Forest. J Geophys Res-Biogeo 112, G02020, doi:10.1029/2006JG000293.

128. Hollinger DY, Aber J, & Dail B (2004) Spatial and temporal variability in forest-atmosphere CO_2 exchange (vol 10, pg 1689, 2004). Global Change Biol 10(11):1961-1961.

129. Allison VJ, Miller RM, Jastrow JD, Matamala R, & Zak DR (2005) Changes in soil microbial community structure in a tallgrass prairie chronosequence. Soil Sci Soc Am J 69(5):1412-1421.

130. Powell TL, et al. (2006) Environmental controls over net ecosystem carbon exchange of scrub oak in central Florida. Agr Forest Meteorol 141(1):19-34.

131. Borken W, Savage K, Davidson EA, & Trumbore SE (2006) Effects of experimental drought on soil respiration and radiocarbon efflux from a temperate forest soil. Global Change Biol 12(2):177-193.

132. Law BE, Thornton PE, Irvine J, Anthoni PM, & Van Tuyl S (2001) Carbon storage and fluxes in ponderosa pine forests at different developmental stages. Global Change Biol 7(7):755-777.

133. Schmid HP, Grimmond CSB, Cropley F, Offerle B, & Su HB (2000) Measurements of CO2 and energy fluxes over a mixed hardwood forest in the mid-western United States. Agr Forest Meteorol 103(4):357-374.

134. Sun G, et al. (2010) Energy and water balance of two contrasting loblolly pine plantations on the lower coastal plain of North Carolina, USA. Forest Ecol Manag 259(7):1299-1310.

135. Noormets A, et al. (2010) Energy and water balance of two contrasting loblolly pine plantations on the lower coastal plain of North Carolina, USA (vol 259, pg 1299, 2010). Forest Ecol Manag 260(1):169-169.

136. Verma SB, et al. (2005) Annual carbon dioxide exchange in irrigated and rainfed maize-based agroecosystems. Agr Forest Meteorol 131(1-2):77-96.

137. Monson RK, et al. (2002) Carbon sequestration in a high-elevation, subalpine forest. Global Change Biol 8(5):459-478.

138. DeForest JL, et al. (2006) Phenophases alter the soil respiration-temperature relationship in an oak-dominated forest. Int J Biometeorol 51(2):135-144.

139. Davis KJ, et al. (2003) The annual cycles of CO_2 and H_2O exchange over a northern mixed forest as observed from a very tall tower. Global Change Biol 9(9):1278-1293.

140. Lipson DA, Wilson RF, & Oechel WC (2005) Effects of elevated atmospheric CO_2 on soil microbial biomass, activity, and diversity in a chaparral ecosystem. Appl Environ Microb 71(12):8573-8580.

141. Powell TL, et al. (2008) Carbon exchange of a mature, naturally regenerated pine forest in north Florida. Global Change Biol 14(11):2523-2538.

142. Clark KL, Gholz HL, & Castro MS (2004) Carbon dynamics along a chronosequence of slash pine plantations in north Florida. Ecol Appl 14(4):1154-1171.

143. Potts DL, Scott RL, Cable JM, Huxman TE, & Williams DG (2008) Sensitivity of Mesquite Shrubland CO_2 Exchange to Precipitation in Contrasting Landscape Settings. Ecology 89(10):2900-2910.

144. Desai AR, Bolstad PV, Cook BD, Davis KJ, & Carey EV (2005) Comparing net ecosystem exchange of carbon dioxide between an old-growth and mature forest in the upper Midwest, USA. Agr Forest Meteorol 128(1-2):33-55.

145. Ma SY, Baldocchi DD, Xu LK, & Hehn T (2007) Inter-annual variability in carbon dioxide exchange of an oak/grass savanna and open grassland in California. Agr Forest Meteorol 147(3-4):157-171.

146. Gough CM, Vogel CS, Schmid HP, Su HB, & Curtis PS (2008) Multi-year convergence of biometric and meteorological estimates of forest carbon storage. Agr Forest Meteorol 148(2):158-170.

147. Wilson KB & Baldocchi DD (2001) Comparing independent estimates of carbon dioxide exchange over 5 years at a deciduous forest in the southeastern United States. J Geophys Res-Atmos 106(D24):34167-34178.

148. Cook BD, et al. (2004) Carbon exchange and venting anomalies in an upland deciduous forest in northern Wisconsin, USA. Agr Forest Meteorol 126(3-4):271-295.

149. Noormets A, Chen J, & Crow TR (2007) Age-dependent changes in ecosystem carbon fluxes in managed forests in northern wisconsin, USA. Ecosystems 10(2):187-203.

150. Sun G, Noormets A, Chen J, & McNulty SG (2008) Evapotranspiration estimates from eddy covariance towers and hydrologic modeling in managed forests in Northern Wisconsin, USA. Agr Forest Meteorol 148(2):257-267.

151. Scott RL, Hamerlynck EP, Jenerette GD, Moran MS, & Barron-Gafford GA (2010) Carbon dioxide exchange in a semidesert grassland through drought-induced vegetation change. J Geophys Res-Biogeo 115, G03026, doi:10.1029/2010JG001348.

152. Falk M, Wharton S, Schroeder M, Ustin S, & U KTP (2008) Flux partitioning in an old-growth forest: seasonal and interannual dynamics. Tree Physiol 28(4):509-520.

153. Navarro M, et al. (2008) Fruit development, not GPP, drives seasonal variation in NPP in a tropical palm plantation. Tree Physiol 28(11):1661-1674.

154. Xiao X, Biradar C, Wang A, Sheldon S, & Chen Y (2011) Recovery of Vegetation Canopy After Severe Fire in 2000 at the Black Hills National Forest, South Dakota, USA. Journal of Resources and Ecology 2(2):106-116.

155. Ciais P, et al. (2005) Europe-wide reduction in primary productivity caused by the heat and drought in 2003. Nature 437(7058):529-533.